Research Journal of Applied Sciences, Engineering and Technology 8(9): 1075-1097, 2014
DOI:10.19026/rjaset.8.1072
ISSN: 2040-7459; e-ISSN: 2040-7467

Submitted: April 08, 2014 Accepted: April 28, 2014 Published: September 05, 2014

Research Article

Spectroscopic Investigation of Pyruvate Formate Lyase-activating Enzyme: A Look into EPR, ENDOR and Mössabuer Spectroscopy

[1]Danilo O. Ortillo and [2]Joan B. Broderick
[1]Department of Chemistry, University of the Philippines Visayas, 5023 Miagao, Iloilo, Philippines
[2]Department of Chemistry and Biochemistry, 103 Chemistry and Biochemistry Building, P.O. Box 173400, Bozeman, MT 59717, USA

Abstract: Electron Paramagnetic Resonance (EPR) and Electron Nuclear Double Resonance (ENDOR) spectroscopies are extremely powerful and versatile methods for the characterization of paramagnetic systems in biology, chemistry and physics. For iron centers in the radical SAM enzymes however, Mössbauer spectroscopy has proven to be both powerful and useful as a complementary spectroscopic technique in determining not just the oxidation states but also the type of iron species present in the catalytic center. The cluster content of the radical SAM protein, Pyruvate Formate-Lyase-Activating Enzyme (PFL-AE), was characterized using EPR and Mössbauer techniques while additional ENDOR analysis helped determine the novel interaction of the co-substrate, S-Adenosylmethionine (SAM or AdoMet) with the Fe-S cluster of PFL-AE. The anchoring role of the Fe-S cluster to the co-substrate derived from the spectroscopic data supports the mechanism where a SAM-based radical species is involved during catalysis.

Keywords: AdoMet, pyruvate formate-lyase-activating enzyme, radical SAM, spectroscopic methods

INTRODUCTION

The chemistry of Fe-S clusters has been thoroughly documented through the years and most of the basic features that we observe with the protein-bound clusters have been determined via *in vitro* studies using model clusters, although generally not in aqueous medium and mostly also in anaerobic conditions (Berg and Holm, 1982; Holm, 1992). However, the model clusters are susceptible to rapid oxidative degradation and require protection by bulky and mostly hydrophobic ligands. Hagen *et al*. (1981) have worked out the ideal conditions under which the simpler clusters can be readily obtained from ferric iron, thiol and sulfide. Simple mononuclear rubredoxin-like $(Fe\ (SR)_4)^{2+}$ complex and the $(Fe_4\ (SR)_{10})^{2+}$ cage complexes are formed when sulfide is not added. The addition of sulfide results to the formation of the (2Fe-2S) and the (4Fe-4S) clusters, with the (4Fe-4S) being the most frequently encountered cluster. A variant of the 4Fe cluster is the (3Fe-4S) cluster, which is a 4Fe cluster with one iron plucked out of one corner. It is readily formed on oxidation of 4Fe clusters which have only three Cys ligands. Such clusters, with one Asp or His or even hydroxyl ligand instead of Cys, are occasionally encountered (Beinert, 2000).

Quantitative EPR studies in conjunction with Mössbauer spectroscopy (Krebs *et al*., 2000) have shown that the $(4Fe\text{-}4S)^{+}$ cluster in Pyruvate Formate-Lyase Activating Enzyme (PFL-AE) is the electron source required for generation of the glycyl radical on Pyruvate Formate-Lyase (PFL). PFL-AE, which functions to generate the catalytically essential glycyl radical of PFL is a member of the "radical-SAM" enzymes super family of enzymes which utilize iron-sulfur clusters and S-adenosylmethionine to initiate radical catalysis (Henshaw *et al*., 2000; Sofia *et al*., 2001).

Electron-Nuclear Double Resonance (ENDOR) studies of Walsby *et al*. (2002a) have likewise shown that the co-substrate AdoMet sits close to the $(4Fe\text{-}4S)^{+}$ cluster of PFL-AE in the enzyme-substrate complex, with the methyl carbon approximately 4-5 Å and the methyl hydrogen approximately 3-4 Å, from the closest iron of the cluster. This close association of AdoMet and the Fe-S cluster has significant implications regarding the catalytic activation of PFL by PFL-AE. Additional ENDOR studies further revealed the coordination of the carboxyl and amino group of the methionine end of AdoMet to the unique iron site of the Fe-S cluster (Walsby *et al*., 2002b).

A combination of spectroscopic methods has led into the discovery of a novel binding motif with important implications to the catalytic mechanism of the radical-SAM super family of proteins, specifically PFL-AE. The purpose of this review will then be:

Corresponding Author: Danilo O. Ortillo, Department of Chemistry, University of the Philippines Visayas, 5023 Miagao, Iloilo, Philippines

- To present the basic principles of EPR, ENDOR and Mössbauer spectroscopy
- To illustrate the application of these spectroscopic methods in elucidating the structure and the function of the iron-sulfur cluster in the radical SAM protein, PFL-AE

Electron paramagnetic spectroscopy: Electron Paramagnetic Resonance spectroscopy (EPR) is a powerful technique used to probe a paramagnetic center by characterizing the interaction of that center with an applied magnetic field. In principle, the method is applicable to any species containing one or more unpaired electrons. An isolated electron without any outside force generates a magnetic field due to its charge and angular momentum. This magnetic moment has no direction in open space unless the electron is placed in an external magnetic field. The interaction of the unpaired spin moment (denoted as $m_s = \pm 1/2$ for a free electron) with the applied magnetic field gives rise to different energy states referred to as the Zeeman effect. The Zeeman Hamiltonian for the interaction of an electron with the magnetic field is given by Eq. (1):

$$\hat{H} = g_e \beta H \hat{S}_z \quad (1)$$

where, g_e is the spectroscopic g-factor of the free electron and is equal to 2.0023193; β is the electron Bohr magneton, $e\hbar/2m_e c$, which has the value of 9.274096 $\pm$ (0.000050) $\times 10^{-21}$ erg/gauss; $\hat{S}_z$ is the spin operator; and H is the applied field strength. The Hamiltonian operates on the electron spin functions α and β corresponding to $m_s = 1/2$ and $-1/2$ respectively. In the presence of a magnetic field, the β spin state has its moment aligned with the field. The lowest energy state in EPR corresponds to $m_s = -1/2$ which is on contrast to nmr where the lowest energy state corresponds to $m_I = +1/2\,(\propto_N)$ because the sign of the charge on the electron is opposite to that of the proton. Therefore, the transition energy is given by Eq. (2):

$$\Delta E = h\nu = g_e \beta H \quad (2)$$

The energy difference between the α and β spin states in magnetic fields of strengths commonly used in the EPR experiment correspond to frequencies in the microwave region. When the energy present in the microwave quantum matches the energy separation between the two spin orientations as shown in Fig. 1, absorption of the microwave energy occurs following the selection rule where $\Delta M_s = \pm 1$ for an EPR transition.

To analyze a paramagnetic molecule, we can imagine a free electron in space with no outside forces acting on it and its magnetic moment is dependent only on its intrinsic spin angular momentum:

$$u \propto g_e S \quad (3)$$

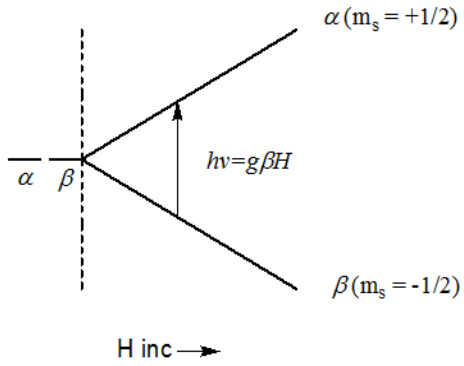

Fig. 1: Splitting of the electronic spin states
The removal of the degeneracy of the α and β electron spin states by a magnetic field

If we place this free electron on to a molecule, the action changes the total angular momentum of the electron because in addition to the intrinsic spin angular momentum S, it now also possesses an orbital angular momentum L. The vector addition of these two quantities results to a different magnetic dipole moment:

$$u \propto g_e S + L \quad (4)$$

In general, the orbital angular momentum is approximately zero for an electron in the ground state which suggests that we only have a spin-only system with an effective *g*-factor equal to g_e. However, mixing of the ground state with excited states via spin-orbit coupling allows the ground state to regain some of its orbital angular momentum:

$$\mu \propto g_e S + s - o\ coupling \quad (5)$$

Assuming the s-o coupling term is proportional to S, we can simplify the equation to:

$$\mu \propto g S \quad (6)$$

which tells us that the magnetic moment of the electron is proportional to the electron spin. The magnitude of the electron spin-orbit coupling contribution depends on the size of the nucleus containing the unpaired electron. Organic free radicals containing H, O, C and N atoms will have a small contribution from spin-orbit coupling resulting to g-factors very close to g_e.

In an EPR spectrometer, a paramagnetic sample is placed in a large uniform magnetic field which splits the α and β ground spin states by ΔE. The separation in energy of the two spin states is variable and depends on the intensity of the magnetic field. It then follows that two instrumental configurations can be conceived for this: first is to set the magnetic field to a certain

Table 1: Microwave frequencies used in EPR spectroscopy

Band	Frequency (GHz)
L	1
S	3
X	9
P	15
K	18
Q	35

value and vary the energy source over the appropriate frequency range. The second configuration fixes the frequency and the intensity of the magnetic field is varied over a relevant range. An EPR experiment is usually carried out using the second configuration at a fixed frequency listed in Table 1 and two common frequencies used are the X-band frequency range (about 9500 MHz or 9.5 GHz) and the Q-band frequency (35 GHz with a field strength of about 12,500 gauss is used). Since the sensitivity of the instrument increases roughly as v^2 and better spectral resolution also results, the higher frequency is to be preferred. However, the use of the Q-band is without any limitations as well. Smaller samples are required so the sensitivity is not as much greater as one would predict from v^2. It is also more difficult to attain higher field homogeneity that is required at higher frequencies.

For samples which are almost always aqueous solutions, dielectric absorption by the solvent becomes an issue as the frequency increases as this result to decreased sensitivity. Solvents with high dielectric constant like water and alcohols strongly absorb microwave power but can still be used when the samples has a strong resonance and is contained in a specially designed cell, usually a narrow sample tube. You can also perform EPR measurements on frozen samples instead especially when the solvent freezes to form a glass. Symmetrical molecules or those that form extensive hydrogen bonding are poor glass formers in which case a mixture of solvents are often used. The sample tube used is also important and a quartz sample tube is preferred if the signal-to-noise ratio is low.

The absorptive curve of the EPR spectrum is displayed as a first derivative due to the electronic circuitry used to acquire the EPR signal. The peak of the absorptive curve which equals the zero crossing of the first derivative relates to the magnetic field for maximum absorption, B_R. Calculating the g value is trivial using the equation below if you have knowledge of the operating frequency of the spectrometer and the intensity of the magnetic field at maximum absorption:

$$g = hv/\beta B_R \quad (7)$$

A limitation to calculating the g value is due to the intrinsic width of the EPR line which can result to difficulty in locating the relevant spectral feature.

An important attribute of EPR is that it allows you to determine the number of paramagnetic centers in a sample by simply comparing the EPR intensity with that of a suitable standard. The procedure involves a double integration of the EPR spectrum of both the unknown sample and the standard and, correction of each double integral for certain instrumental parameters. The relationship between the two Corrected Double Integral (CDBLI) to the concentration of spins is shown below (Palmer, 2000):

$$[spins]_{unknown} = spins_{std} x \frac{CDBLI(unknown)}{CDBLI(Standard)} \quad (8)$$

This procedure is straightforward for an S = 1/2 system which is exemplified by the reduced Fe-S cluster of Pyruvate Formate Lyase-Activating Enzyme (PFL-AE) and the subsequent glycyl radical formed on the activated Pyruvate Formate Lyase (PFL) protein.

The activase PFL-AE from *E. coli* has a molecular mass of 28 kDa and is a radical SAM enzyme (Conradt *et al*., 1984). Initially isolated aerobically from non-over expressing *E. coli* cells, it showed an absorption spectrum indicating the presence of a covalently bound cofactor. Wong *et al*. (1993) have shown that the catalytic activity of PFL-AE was totally dependent on the presence of exogenous iron in the assay which was the first indication of the role of iron in the glycyl radical generation. Isolation of PFL-AE in its native state under strictly anaerobic conditions led to the identification of the presence of an iron-sulfur cluster. EPR first-derivative spectra were obtained at X-band at 12 K for the $(3Fe\text{-}4S)^+$ and $(4Fe\text{-}4S)^+$ clusters. The double integrals of the EPR signals were evaluated by using a computer on-line with the spectrometer and spin concentrations in the protein samples were determined by calibrating double integrals of the EPR spectra recorded under non-saturating conditions:

- With a standard sample of 0.1 mM Cu (II) and 1 mM EDTA solution for the cluster signals
- With a 1.04 mM K_2 $(SO_3)_2NO$ solution for the glycyl radical signals. The concentration of the K_2 $(SO_3)_2NO$ standard was determined using the optical extinction coefficient

Broderick *et al*. (2000) have shown that the purified PFL-AE without the addition of Dithiotrietol (DTT) contain primarily a $(3Fe\text{-}4S)^+$ cluster as confirmed by a combination of UV-visible, EPR and resonance Raman spectroscopic methods. EPR spectrum of the $(3Fe\text{-}4S)^+$ shows a nearly isotropic signal centered around 3500 Gauss (g = 2.17) shown in Fig. 2. An isotropic spectrum is a single symmetrical line due to the g-factor being invariant with

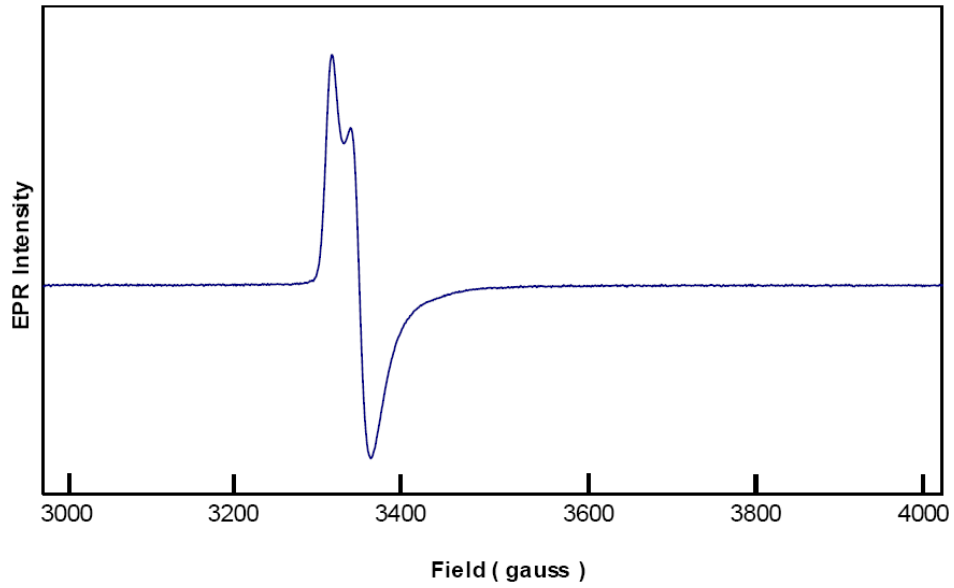

Fig. 2: EPR spectrum of as-isolated PFL-AE
X-band EPR spectrum of PFL-AE $(3Fe\text{-}4S)^{+}$ from as-isolated protein: 7.41% (based on 97.9 μM spin for 1321 μM protein with 3.70 mol Fe/mol PFL-AE), g = 2.17; Conditions of measurement: T = 12 K, microwave power = 20 μW, microwave frequency = 9.49 GHz, modulation amplitude = 10.084 G; Single scan

direction with all of the principal g-factors being equal $(g_x = g_y = g_z)$.

In the dithionite-reduced form of PFL-AE, all cluster types were converted into the (4Fe-4S) form. The (4Fe-4S) cluster was expected to be the catalytically relevant cluster, which is generated under the reducing conditions present in the activity assay. Cheek and Broderick (2001) have shown that PFL-AE purified under anaerobic reducing conditions in the presence of DTT yield essentially EPR-silent clusters, presumably in the $(4Fe\text{-}4S)^{2+}$ state, which can be readily reduced to $(4Fe\text{-}4S)^{+}$, the cluster that is responsible for providing the electron necessary for AdoMet dependent glycyl radical generation on PFL. In the absence of AdoMet, the reduced cluster gives a rhombic EPR signal shown in Fig. 3A (g = 2.02, 1.94, 1.88) which is typical when all the g-factors differ $(g_x \neq g_y \neq g_z)$. The principal g-factors can be determined from the derivative spectrum by noting the field positions for both the maximum and minimum of the absorption-shaped signals $(g_z \; and \; g_x)$ as well as the crossover (g_y) of the center of the derivative-shaped signal.

Henshaw *et al*. (2000) have demonstrated that the $(4Fe\text{-}4S)^{+}$ is indeed the catalytically active cluster of PFL-AE and that it donates the electron required for reductive cleavage of AdoMet. The reduced cluster in the presence of AdoMet shows a nearly axial signal shown in Fig. 3B which is a result of one of the unique axis being different from the other two $(g_x = g_y \neq g_z)$. The unique g-factor is parallel with this axis $(g_z = g_{\parallel})$ while the remaining two axes are perpendicular to it, $(g_x = g_y = g_{\perp})$. The g-factors of the cluster (g = 2.01, 1.88, 1.87) is obtained by noting the magnetic field for the minor-shaped inflection $(g_{\parallel})$ and the midpoint of the derivative-shaped signal $(g_{\perp})$.

Spin quantitation experiment and generation of the glycyl radical: Pyruvate formate-lyase from *E. coli* is a glycyl radical-containing enzyme that catalyzes the first committed step in anaerobic glucose metabolism by converting pyruvate and coenzyme A (coA) into formate and acetyl-coA (Knappe *et al*., 1974). It is a dimeric enzyme of 170 kDa composed of identical units where the inactive enzyme is activated posttranslationally to contain a glycyl radical at position 734 (Wagner *et al*., 1992; Knappe *et al*., 1993). The glycyl-734 radical in the sequence $_{731}$RVSGY$_{735}$ of PFL has been characterized by isotope labeling and EPR spectroscopy (Wagner *et al*., 1992). Abstraction of the pro-*S* hydrogen from the C-2 of Gly734 is catalyzed by its activase (PFL-AE) and proceeds with concomitant cleavage of AdoMet into methionine and 5'-deoxyadenosine as shown in Fig. 4. AdoMet does not function catalytically in this process, but rather as a substrate in an irreversible reaction (Frey, 2001).

Henshaw *et al*. (2000) have reported that each $(4Fe\text{-}4S)^{1+}$ cluster of PFL-AE under conditions of limiting reductant is capable of generating a single glycyl radical on PFL. Their results provided the first direct quantitative spectroscopic evidence that the $(4Fe\text{-}4S)^{1+}$ of PFL-AE is the catalytically relevant cluster. The glycyl radical spectrum of PFL was recorded at

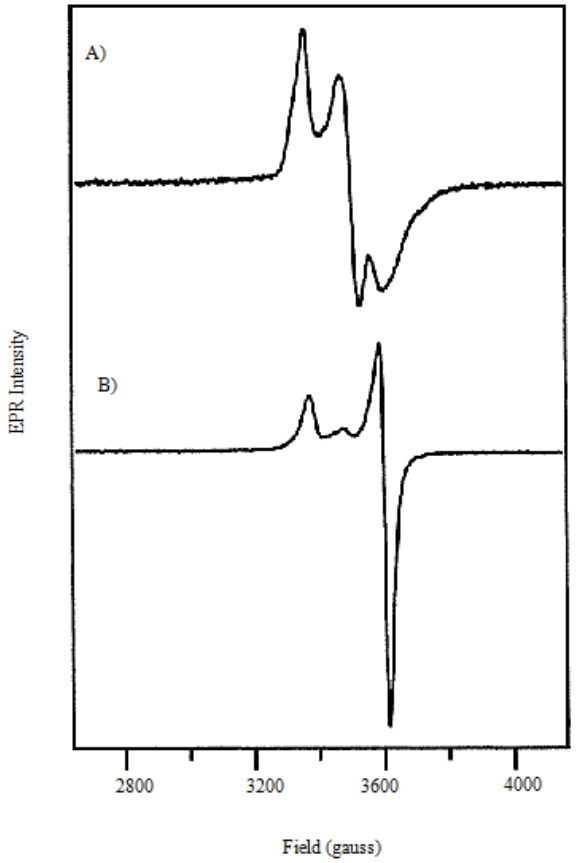

Fig. 3: EPR spectra of as-isolated reduced and as-isolated reduced with SAM PFL-AE $(4Fe\text{-}4S)^{+}$ cluster
X-band EPR spectra of PFL-AE photoreduced with deazariboflavin (A) PFL-AE (0.7 mM) photo reduced for 1 h. The signal accounts for 197 μM $(4Fe\text{-}4S)^{+}$ based on EPR spin quantitation, and has been multiplied by 3 for comparison purposes. (B) PFL-AE (0.78 mM) photo reduced for 1 h, followed by addition of two molar equivalents of AdoMet. The signal accounts for 416 μM $(4Fe\text{-}4S)^{+}$ based on EPR spin quantitation. Conditions: T = 12 K, power = 20 μW, gain = 2×10^{4}, frequency = 9.483 (A) or 9.476 (B), modulation amplitude = 8.231 (A) or 9.571 (B)

60 K, a temperature at which the $(4Fe\text{-}4S)^{+}$ signal of PFL-AE is not observed. The rhombic-shaped EPR spectrum of PFL can be generated using turnover conditions for PFL-AE by using a limited amount of reductant. The EPR silent $(4Fe\text{-}4S)^{2+}$ is converted to the reduced $(4Fe\text{-}4S)^{+}$ cluster via photoreduction by illuminating the samples at certain times after which AdoMet was then added. The sample was split into two where an equimolar amount of PFL was added to one half of the sample in the dark. EPR spectra were recorded to detect the $(4Fe\text{-}4S)^{+}$ (Fig. 5A) and glycyl radical in these samples (Fig. 5B). Spin quantitation of the axial signal of the reduced $(4Fe\text{-}4S)^{+}$ cluster correlates to the amount of glycyl radical generated and plotted on Fig. 6. The multiplet signal of the glycyl radical shows a g value of 2.007 with a splitting value of about 17 Gauss.

The purification of PFL-AE containing primarily $(3Fe\text{-}4S)^{+}$ clusters implies a labile fourth iron site and is consistent with the observation that only three cysteines have been implicated in cluster coordination. These three cysteines exist in a CX_3CX_2C motif that is common to all of the AdoMet dependent Fe-S enzymes for which a sequence has been determined (Külzer *et al*., 1998). The identity of the fourth ligand to the (4Fe-4S) cluster in PFL-AE was previously unknown. However, by analogy to aconitase, in which substrate coordinates to the unique iron site and solvent binds in the absence of substrate or product, it was reasonable to propose that exogenous ligands such as water or substrate may bind to the unique labile iron site in PFL-AE. ENDOR Spectroscopy coupled with EPR eventually paved the way in determining the ligand to the labile fourth Fe site.

Mössbauer spectroscopy: Mössbauer spectroscopy has developed into a powerful tool used to investigate the electronic structure of compounds with high resolution after the discovery of recoilless nuclear gamma resonance by Rudolf Mössabuer in 1958. The Mössbauer effect, which requires a nucleus with low-lying excited states, has been observed for 43 elements but by far, the most utilized nucleus is ^{57}Fe, a stable isotope with 2.2% natural abundance. In ^{57}Fe Mossbauer spectroscopy, we observe transitions between the nuclear ground state of ^{57}Fe (nuclear spin $I_g = 1/2$; nuclear g factor, $g_g = 0.181$) and a nuclear excited state at 14.4 KeV ($I_e = 3/2$; $g_e = -0.106$,

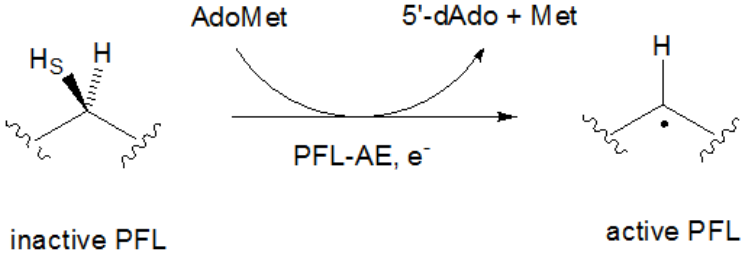

Fig. 4: Abstraction of pro-S hydrogen at glycine 734 (reductive cleavage of AdoMet by PFL-AE during the activation of PFL)

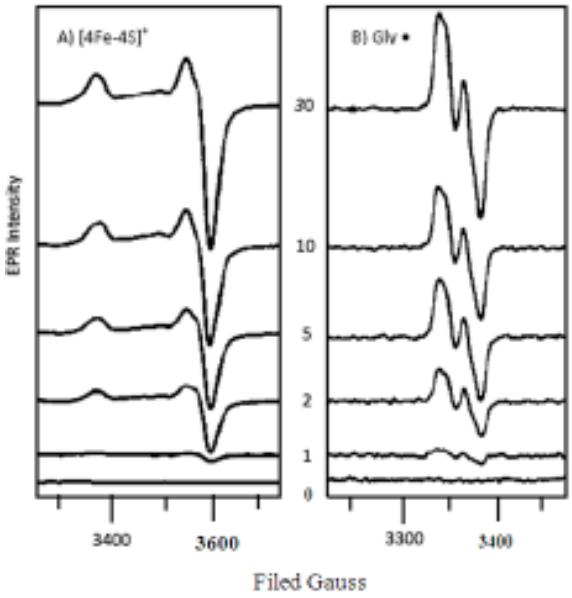

Fig. 5: Spin quantitation experiment
X-band EPR spectra of photoreduced PFL-AE before (A) and after addition of PFL (B); Panel A: EPR spectra recorded after photoreduction of PFL-AE in the presence of 5-deazariboflavin at 0, 1, 2, 5, 10 and 30 min, respectively; Conditions of measurement: T = 12 K, microwave power = 2 mW, microwave frequency = 9.48 GHz, modulation amplitude, 10.084, single scan, protein concentration = 200 uM; Panel B: EPR spectra of photoreduced PFL-AE samples after addition of PFL; Conditions of measurement: T = 60 K, microwave power = 20 uW, microwave frequency = 9.48 GHz, modulation amplitude = 5.054, single scan, protein concentration = 100 uM

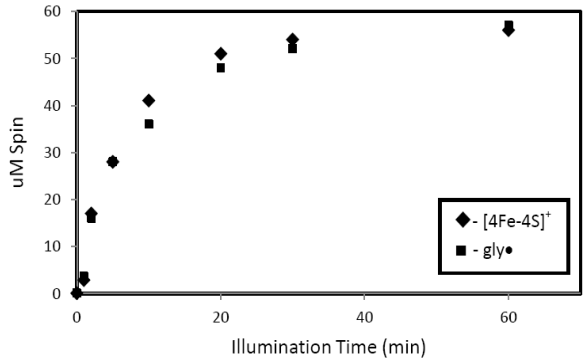

Fig. 6: Spin quantitation data
Spin quantitation of the EPR spectra for $(4Fe\text{-}4S)^+$ (A) and glycyl radical (B) as a function of illumination time; Included are additional data points at 20 and 60 min

nuclear quadrupole moment Q). For the bare nucleus, the nuclear ground state and excited states would exhibit twofold and fourfold degeneracies respectively and only a single Mössbauer transition would be observed. Mossbauer spectroscopy is traditionally preformed with a radioactive ^{57}Co source. While it can well stand on its own, the power of this technique is substantially increased when it is applied in combination with EPR spectroscopy.

Recoil-free absorption of γ rays: The Mössbauer effect is a recoil-free resonant absorption of a γ-quanta by a nuclei of the same kind as the emitter. A free nucleus can undergo a transition from an excited state with energy E_e to a ground state E_g by emission of a γ-quanta. The nucleus suffers a recoil during the emission and the energy of this quantum is given as:

$$E_\gamma^0 = E^0 - E_R \quad (9)$$

E^0 is the nuclear transition energy and can be written as:

$$E^0 = E^e - E^g \quad (10)$$

E_R is the recoil energy of the nucleus after the emission of the γ-quantum and is expressed as:

$$E_R = \frac{E_\gamma^{0^2}}{2Mc^2} \approx \frac{E^{0^2}}{2Mc^2} \quad (11)$$

where,
M = The nuclear mass
c = The speed of light (Schünemann and Winkler, 2000)

The curve on the right half of the Fig. 7 shows the distribution of the γ-ray energies necessary for absorption. The shaded area shows the region where the γ-ray energy from the source match the energy required for absorption by the sample. Since the nuclear levels are quantized, there is accordingly a low probability

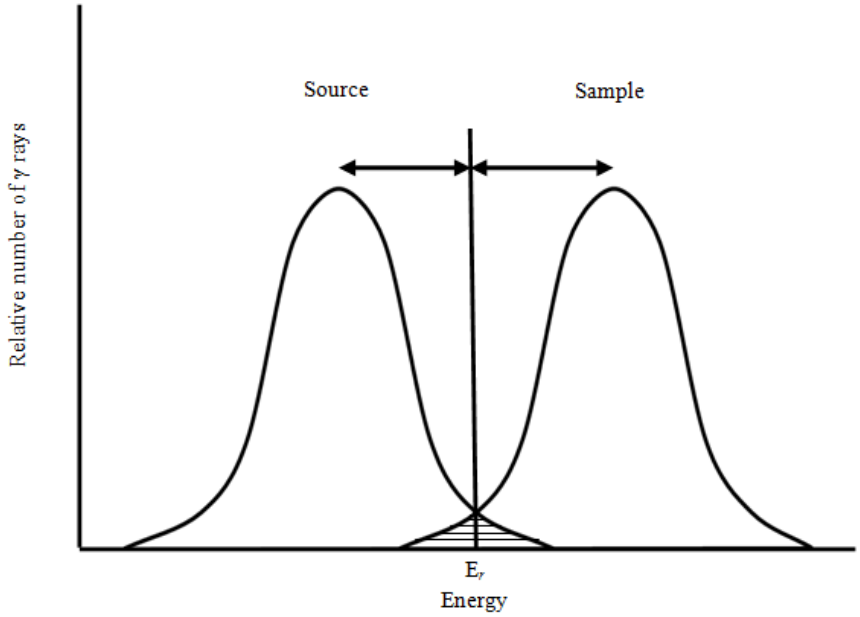

Fig. 7: Distribution of energies of emitted and absorbed γ-rays
The curve on the right half shows the distribution of γ-ray energies necessary for absorption. As indicated by the shaded region, there is only a slight probability that the γ-ray from the source will match that required for absorption to induce a nuclear transition in the sample

that the γ-ray from the source will be absorbed to give a nuclear transition in the sample (Drago, 1977). The main cause for the no matching of γ-ray energies is the recoil energy. As the same amount of energy due to recoil is lost during absorption, it is necessary to design an experiment that will allow you to determine the resonance absorption between two nuclei of the same kind. In other words, the shift of E_γ has to be balanced by an energy equivalent of $2E_R$. To accomplish this, we can:

- Make use of the Doppler effect in order to increase E_γ and mount the source on an ultracentrifuge. Resonance absorption will occur if the Doppler energy:

  $E_D = E_\gamma V/c$ reaches $2E_R$

- Use the recoil-free method by embedding the nucleus in a crystal lattice. The recoil energy is absorbed by the whole crystal lattice where the recoil energy shows a dependence on the mass of the whole lattice, $M_{lattice}$ and not the mass M of the nucleus:

$$E_R^{Moss} = \frac{E_\gamma^2}{2M_{lattice}c^2} \cong 0 \quad (12)$$

Because $M_{lattice}$ is much larger than the nuclear mass M, the recoil energy is negligible and resonance absorption takes place (Schünemann and Winkler, 2000).

Experimental set up and spectral line shape: ^{57}Fe-Mossbauer spectroscopy is in transmission geometry using a single-line source with energy E^0_{source} and a single-line absorber with energy $E^0_{absorber}$ as shown in Fig. 8. In a transmission experiment, the γ-rays emitted by the source are registered by a detector after they have passed the absorber. To determine the energy spectrum of the absorber nuclei, the energy of the emitted γ-rays is modulated by moving the source relative to the absorber with a velocity V where $E_\gamma = \left(1 + \frac{V}{c}\right) E^0_{source}$ (Drago, 1977; Schünemann and Winkler, 2000). Under resonance condition, the Doppler energy shift matches the energy difference between the emitted source and the absorption line of the absorber (Fig. 9).

Hyperfine structure of Fe-mossbauer spectra: The Hamiltonian of the nucleus can be described by a sum of the unperturbed nuclear Hamiltonian and a perturbation caused by the hyperfine interactions which are present at the nucleus of the Mossbauer isotope:

$$\hat{H}_N = \hat{H}_N^0 + \hat{H}^{hf} = \hat{H}_N^0 + \hat{H}_1(E0) + \hat{H}_M(M1) + \hat{H}_Q(E2) + \cdots \quad (13)$$

$E0$ denotes the electrical monopole interaction which causes the isomer shift, $E2$ stands for the electric

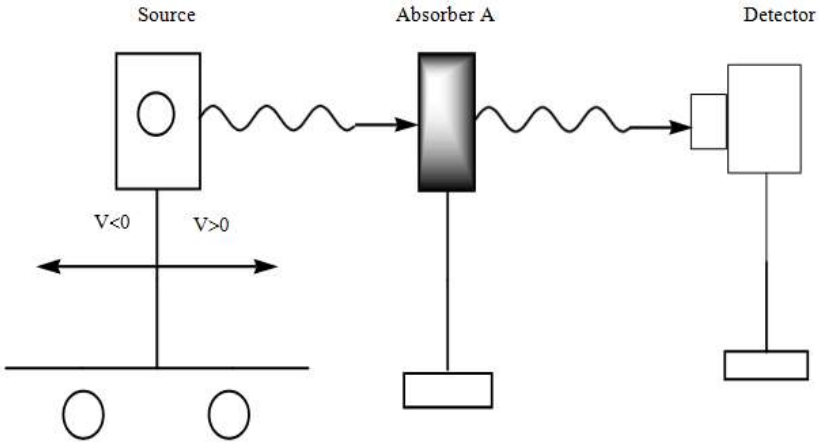

Fig. 8: Mössbauer experimental setup
Schematic illustration of mössbauer spectroscopy in transmission geometry using a single-line source and a single-line absorber; The movement of the source with velocity V modulates the energy of the emitted γ-quanta

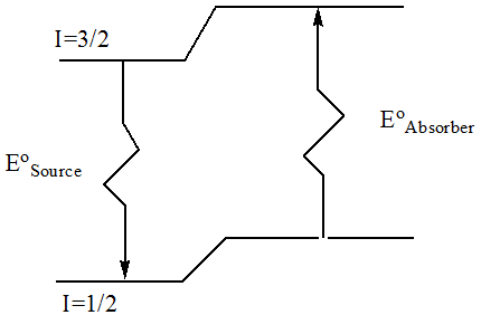

Fig. 9: Shift of the nuclear energy levels
Shift of the nuclear energy levels of ^{57}Fe in the source and the absorber

quadrupole interaction which manifests itself in the quadrupole splitting leading for the case of ^{57}Fe to a two-line Mossabuer pattern. *M*1 denotes the magnetic dipole interaction, which leads for ^{57}Fe to a magnetically split six-line pattern (Schünemann and Winkler, 2000).

Isomer shift: The electric monopole interaction (Schünemann and Winkler, 2000) is proportional to the s-electron density at the iron nucleus $|\varphi(0)|^2$ and can be expressed by:

$$E = \tfrac{2}{3}\pi \cdot Z^2 e^2 |\varphi(0)|^2 \cdot \langle r^2 \rangle \quad (14)$$

With $\langle r^2 \rangle$ being mean-square nuclear radius and Ze the nuclear charge. The nuclear radius for the ground state is different than the excited nuclear states with energies $E^{g'}$ and $E^{e'}$ respectively. The energy shift for a nuclear transition is given as:

$$\delta E = E^{e'} - E^{g'} - E^0 = \tfrac{2}{3}\pi \cdot Z^2 e^2 |\varphi(0)|^2 \cdot [\langle r^2 \rangle^e - r2g \quad (15)$$

In general, the source and absorber nuclei are embedded in different matrices, which leads to different s-electron densities at the source and the absorber nuclei (Fig. 9). Therefore, the isomer shift δ can be expressed as:

$$\delta = \delta E_{source} - \delta E_{absorber} \quad (16)$$

The electric quadrupole splitting: The electric quadrupole interaction is described by the Hamiltonian:

$$\hat{H}(E2) = \frac{eQV_{zz}}{4I(2I-1)}\left[3\hat{I}_z^2 - I(I+1) + (\hat{I}_x^2 - \hat{I}_y^2)\right] \quad (17)$$

where, Q is the nuclear quadrupole moment and I the nuclear spin of the nuclear state with $\hat{I}_x^2, \hat{I}_y^2, \hat{I}_z^2$ as the corresponding spin operators. Since the electric quadrupole moment of the nuclear ground state of ^{57}Fe with $I_g = 1/2$ is zero, the quadrupole interaction does not affect the ground state, but splits the first excited nuclear state with I_e = 3/2 into two sublevels. As a result, ^{57}Fe produces a two-line Mossbauer absorption pattern (Fig. 10) with a corresponding quadrupole splitting ΔE_Q given by Schünemann and Winkler (2000):

$$\Delta E_Q = \frac{1}{2} eQV_{zz}\sqrt{1 + \frac{\eta^2}{3}} \quad (18)$$

The magnetic splitting: The Hamiltonian for the magnetic interactions contains two contributions. The first contribution comes from the nuclear Zeeman effect which couples the magnetic moment of the nucleus to the external magnetic field, $\overrightarrow{B_0}$. The second contribution arises from the interaction with an internal magnetic hyperfine field.

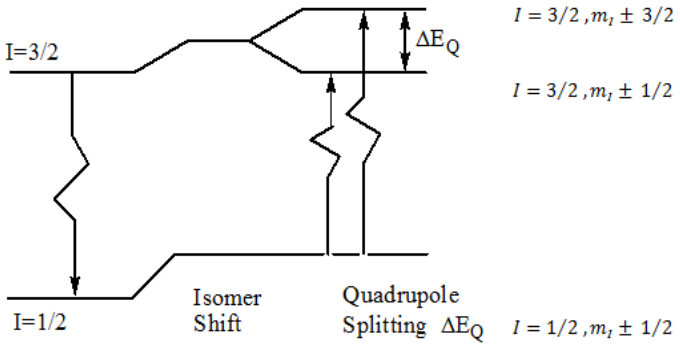

Fig. 10: Quadrupole splitting of the excited state
Quadrupole splitting of the ^{57}Fe excited state and shift of the nuclear states by the electric monopole interaction that gives rise to the isomer shift; The excited nuclear state is split into twofold degenerate sublevels which explains the observed two-line pattern

In the case of magnetic materials, in addition to the external field, an internal magnetic hyperfine field B_{hf} is present. For most cases, the internal field is much higher than external magnetic fields. Metallic iron exhibits a magnetic hyperfine fine field or about -33T at 300 K and is oriented antiparallel to the magnetization of the sample (Schünemann and Winkler, 2000).

^{57}Fe content of PFL-AE: Iron and protein content of the ^{57}Fe-enriched PFL-AE show an iron to protein monomer ratio of 1.3 which is lower than the 2.8 Fe/protein monomer reported for the enzyme purified from bacteria grown in terrific broth with naturally available Fe (Krebs *et al*., 2000). Since the ^{57}Fe-enriched PFL-AE was isolated from bacteria grown in a defined medium, this observed difference in Fe content may suggest inefficient incorporation of the Fe cluster under suboptimal growth conditions. EPR and UV-visible spectroscopic properties of ^{57}Fe-enriched PFL-AE are essentially identical to those of PFL-AE isolated from bacteria grown with naturally available Fe. The specific activity of the ^{57}Fe-enriched PFL-AE containing 1.3 Fe/protein monomer (48 U/mg) is approximately half that for un-enriched PFL-AE containing 2.65 Fe/protein monomer (95 U/mg). These observations indicate that the only difference between ^{57}Fe-enriched and un-enriched PFL-AE is the absolute quantity of iron incorporated, not the form in which it is incorporated.

Fe-S cluster composition in dithionite reduced-PFL-AE: Mössbauer spectroscopy obtained at various temperatures and applied fields of anaerobically purified ^{57}Fe-enriched PFL-AE in two different states (as-isolated and dithionite-reduced) showed that both samples contain mixtures of Fe species. The observed spectra are super positions of the various spectra of the different species contained in the samples and a self-consistent iterative approach was employed to obtain a set of parameters for the different species such that all the spectra recorded under different conditions can be explained by the same set of parameters.

The 4.2 K Mössbauer spectrum of a dithionite-reduced PFL-AE sample (Fig. 11), recorded in a magnetic field of 50 mT oriented parallel to the γ-beam, displays an intense central quadrupole doublet (marked by a bracket), a broad absorption peak at ~2.8 mm/sec and weak absorptions between -2 and +2.5 mm/sec. The features observed are associated with three spectral component srepresenting three different Fe species. The broad absorption peak at ~2.8 mm/sec is the high-energy line of a quadrupole doublet (shown as a solid line in Fig. 11), the parameters and shape of which are indicative of adventitiously bound high-spin Fe (II). Removal of the contribution of the adventitious Fe (II) which accounts for about 25% of the total Fe absorption from the raw data, reveals the spectrum arising from the Fe-S clusters (Fig. 12A). The central quadrupole doublet, accounting for 66% of the total Fe absorption, is best simulated with two overlapping quadrupole doublets (dashed line in Fig. 12A). The parameters used in the simulation are typical for a $(4Fe\text{-}4S)^{2+}$ clusters and are listed in Table 2 (Middleton *et al*., 1978, 1980; Trautwein *et al*., 1991).

All $(4Fe\text{-}4S)^{2+}$ clusters, without exception, have an $S = 0$ ground state, resulting from the anti-ferromagnetic coupling of the two valence-delocalized Fe- (II) Fe (III) units. For the spectrum in Fig. 12C, the spin state of the species associated with the central doublet is obtained using a spectrum recorded in a strong external field of 8 T at 4.2 K of the dithionite-reduced PFL-AE. The solid line plotted over the data in Fig. 11C is simulated using the parameters obtained for the central doublet from the weak-field spectrum and assuming diamagnetism. The result is a strong agreement between the simulation and the central portion of the experimental spectrum which confirms that the central doublet is arising from a diamagnetic species, the $(4Fe\text{-}4S)^{2+}$ cluster.

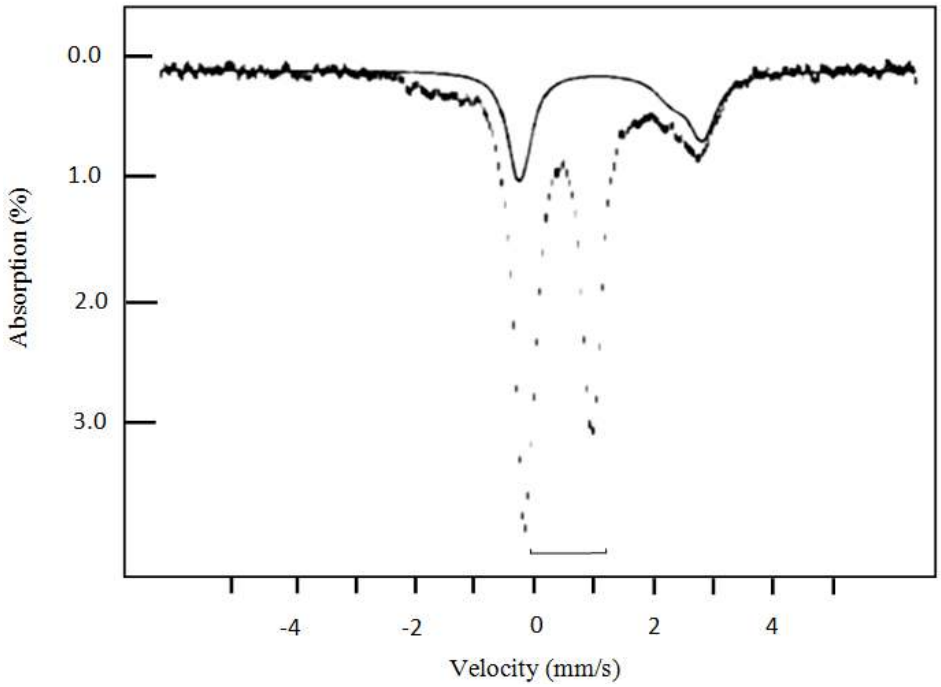

Fig. 11: Mössbauer spectra of dithionite-reduced native PFL-AE
Mössbauer spectrum of dithionite-reduced native PFL-AE recorded at 4.2 K in a magnetic field of 50 mT applied parallel to the γ-beam; The bracket indicates the positions of the quadrupole doublet arising from the $(4Fe\text{-}4S)^{2+}$ cluster; The solid line is the theoretical simulation of adventitiously bound Fe (II) using two quadrupole doublets; Doublet 1 accounts for 17% total absorption with parameters: δ = 1.28 mm/sec, ΔE_Q = 3.07 mm/sec; Doublet 2 accounts for 8% absorption with parameters: δ = 1.10 mm/sec, ΔE_Q = 2.42 mm/sec

Table 2: Temperature-dependent mössbauer parameters of the Fe-S clusters in native PFL-AE[a]

		T (K)		
		4.2	113	170
$(4Fe\text{-}4S)^{2+}$	δ (mm/sec)	0.45 (2)	0.44 (2)	0.42 (2)
Site 1	ΔE_Q (mm/sec)	1.15 (4)	1.13 (4)	1.10 (4)
	η	0.03		
Site 2	δ (mm/sec)	0.45 (2)	0.44 (2)	0.42 (2)
	ΔE_Q (mm/sec)	1.00 (4)	0.83 (4)	0.80 (4)
	η	0.70		
$(2Fe\text{-}2S)^{2+}$	δ (mm/sec)	0.29 (2)	0.26 (2)	0.23 (2)
	ΔE_Q (mm/sec)	0.58 (4)	0.58 (4)	0.58 (4)
	η	0		

Values in parentheses are uncertainties in terms of the least significant digit

Figure 12B shows a spectrum of the dithionite reduced PFL-AE recorded at 170 K in the absence of an applied field where the contribution of the adventitiously bound Fe (II) has been removed from the spectrum shown. The paramagnetic component observed at 4.2 K has collapsed into quadrupole doublets at this temperature. To demonstrate that the high temperature spectrum is in agreement with the low-temperature data, the central doublet (long-dashed line in Fig. 12B for the $(4Fe\text{-}4S)^{2+}$ cluster) was simulated and according to the intensities determined from the low-temperature spectra (66% for the $(4Fe\text{-}4S)^{2+}$ and 12% for the $(4Fe\text{-}4S)^{+}$), the plotted sum (solid line) over the experimental spectrum is in good agreement. This indicates that both the high-temperature and low-temperature Mössbauer data are consistent except for the adventitiously bound Fe (II) because only (4Fe-4S) clusters are present in the dithionite-reduced PFL-AE.

The remaining component having absorption extending from -2 to 2.5 mm/sec, which accounts for 12% of the total Fe absorption, is attributed to a paramagnetic species, the reduced $(4Fe\text{-}4S)^{+}$ cluster with an $S = 1/2$ ground state. Mössbauer spectra of such clusters consist of two equal intensity subspectra representing a valence-delocalized Fe (II) Fe (III) pair and a diferrous pair (Middleton *et al*., 1978; Trautwein *et al*., 1991). Parameters obtained for the $(4Fe\text{-}4S)^{+}$

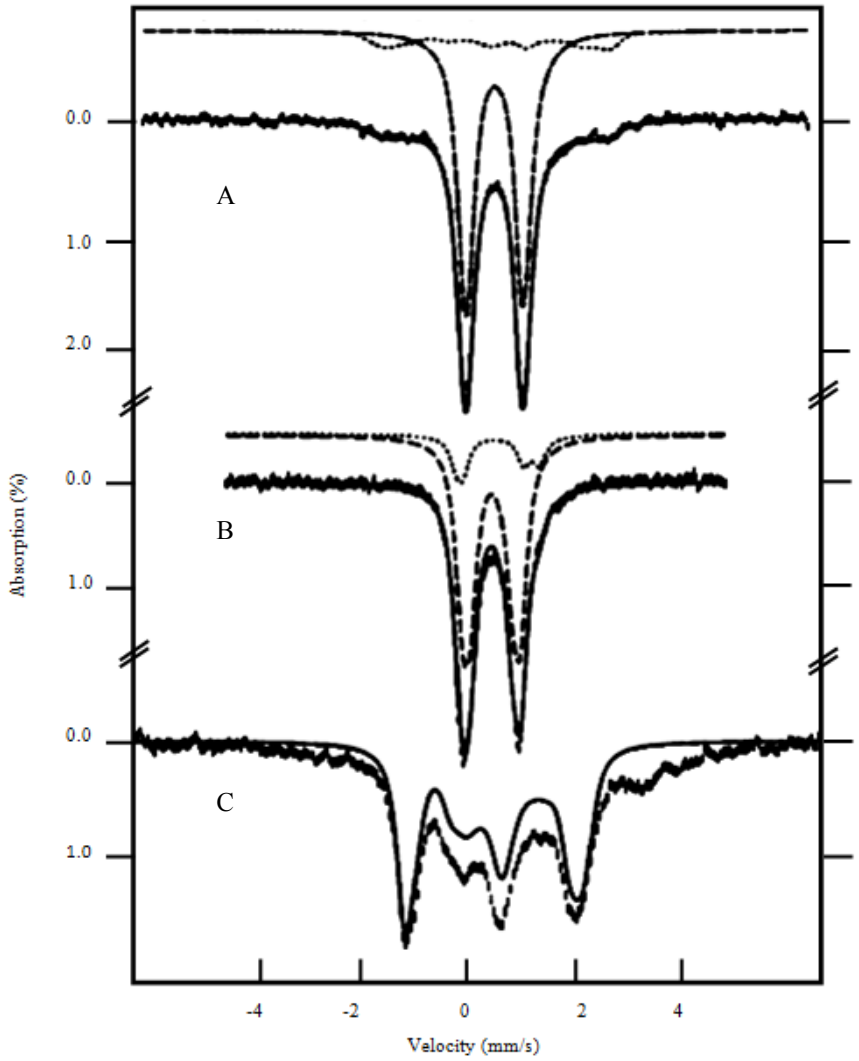

Fig. 12: Mössbauer spectra of dithionite-reduced PFL-AE with adventitiously bound Fe (II) removed
Mössbauer spectra of dithionite-reduced PFL-AE recorded with contributions from the adventitiously bound Fe (II) removed (A and B); Spectra A was recorded at 4.2 K in a parallel field of 50 mT; Spectra B was recorded at 170 K in the absence of applied field (B); The soild lines in A and B are summations of theoretical simulations of the $(4Fe\text{-}4S)^{2+}$ (dashed lines, 66% of total Fe absorption) and the $(4Fe\text{-}4S)^{+}$ (dotted lines, 12%) clusters; Spectra C was recorded at 4.2 K in a parallel field of 8 T; The solid line in C is the theoretical simulation of the $(4Fe\text{-}4S)^{2+}$ cluster with the assumption the cluster is diamagnetic

cluster of *Bacilluss tearothermophilus* ferredoxin (Middleton *et al*., 1978) were used to simulate a spectrum for comparison with this component (dotted line in Fig. 12A). The magnetic splitting and shape of the paramagnetic component in PFL-AE agree well with the simulation where addition of the simulated $(4Fe\text{-}4S)^{+}$ spectrum (12%) with the least-squares fit spectrum for the $(4Fe\text{-}4S)^{2+}$ cluster (66%) generates the solid line which is in good agreement when overlaid with the experimental spectrum shown in Fig. 12A.

EPR measurements confirms the presence of a small quantity of $(4Fe\text{-}4S)^{+}$ cluster in the dithionite-reduced PFL-AE. An X-band EPR spectrum of a dithionite-reduced PFLAE prepared in parallel with the Mössbauer sample displays an axial $S = 1/2$ signal with g values at 2.01 and 1.94. This signal is very similar to that reported for the dithionite-reduced reconstituted PFL-AE (Külzer *et al*., 1998) and double integration of this signal yields a spin quantitation of 0.03-0.04 spin/protein monomer, a value that is consistent with the Mössbauer finding of ~0.04 $(4Fe\text{-}4S)^{+}$ cluster per protein monomer.

Cluster composition in as-isolated PFL-AE: Mössbauer spectrum of the as-isolated PFL-AE recorded at 4.2 K in a parallel applied field of 50 mT shows at least three discernable spectral components. The major component, which accounts for 66% of the Fe absorption, displays magnetic hyperfine interactions

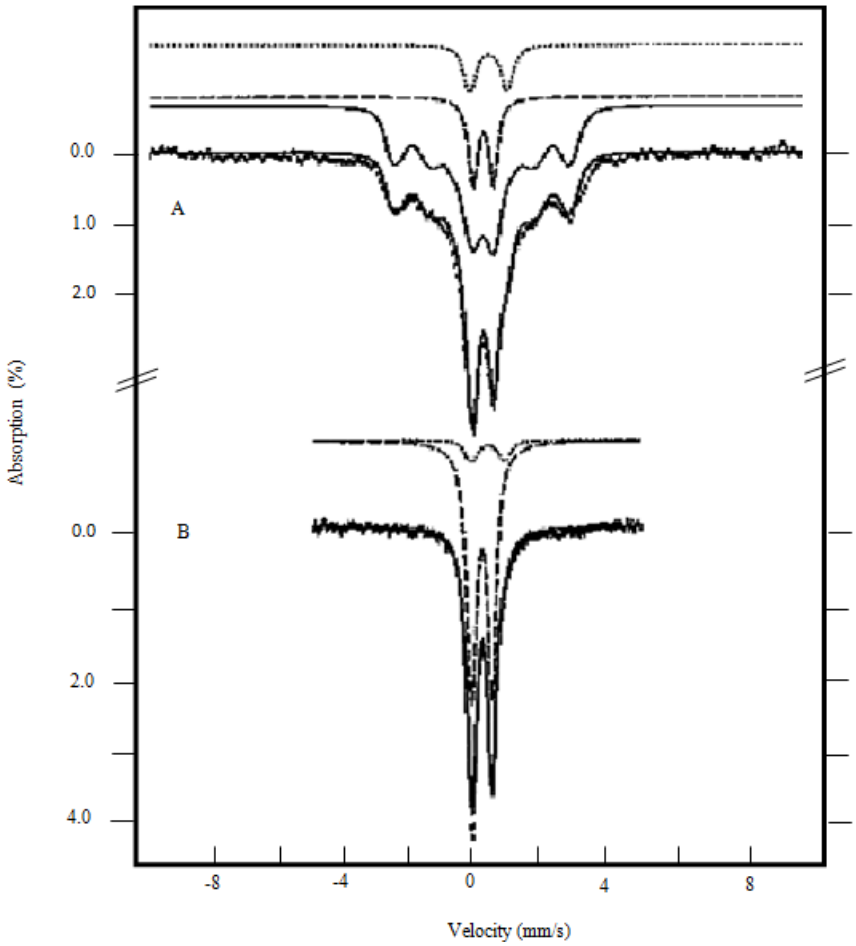

Fig. 13: Mössbauer spectra of an aerobically purified native PFL-AE
Mössbauer spectra of an aerobically purified native PFL-AE; The spectra were recorded at 4.2 K in a parallel field of 50 mT (A) and 170 K in zero field (B); The solid line overlaid with the experimental spectrum in A is the sum of the theoretical simulations of the cuboidal $(3Fe\text{-}4S)^{+}$ (soild line above the experimental spectrum, 66%), $(2Fe\text{-}2S)^{2+}$ (dashed line, 12%) and $(4Fe\text{-}4S)^{2+}$ (dotted line, 8%) clusters; The solid line in B is the sum of the quadrupole doublets arising from the $(4Fe\text{-}4S)^{2+}$ cluster (dotted line above the experimental spectrum) and from the cuboidal $(3Fe\text{-}4S)^{+}$ and $(2Fe\text{-}2S)^{2+}$ (dashed line) clusters

with absorption extending from -2 to 3 mm/sec. This component is composed of three equal intensity sub-spectral components and exhibits field-orientation and field-strength dependence consistent with an $S = ½$ electronic system. At temperatures above 77 K, this magnetic component collapses into a quadrupole doublet (Fig. 13B) with parameters $\delta = 0.23$ mm/sec and $\Delta E_Q = 0.58$ mm/sec at 170 K, typical of tetrahedral sulfur-coordinated high-spin Fe (III). All these features are characteristic of the all-ferriccuboidal $(3Fe\text{-}4S)^{+}$ cluster (Broderick *et al*., 2000).

A second spectral component accounting for 12% of the total Fe absorption is a sharp quadrupole doublet observed at 4.2 K originating from a diamagnetic species with parameters characteristic of $(2Fe\text{-}2S)^{2+}$ clusters (Ferreira *et al*., 1994; Trautwein *et al*., 1991). Removal of the contributions of the $(3Fe\text{-}4S)^{+}$ and $(2Fe\text{-}2S)^{2+}$ clusters from the raw data reveals a third component identical to that of the $(4Fe\text{-}4S)^{2+}$ cluster observed in the dithionite-reduced PFL-AE. The high-energy line of this doublet can be seen as a shoulder at ~1 mm/sec in the raw data and is estimated to account for ~8% of the total Fe absorption. A sum of the three components (the $(3Fe\text{-}4S)^{+}$, $(2Fe\text{-}2S)^{2+}$ and $(4Fe\text{-}4S)^{2+}$) yields the solid line plotted over the data in Fig. 13A. Although the agreement between the experiment and the simulated sum spectrum is reasonable, approximately 14% of the Fe absorption remains not accounted for. Spectra recorded at strong applied field reveal the presence of a fourth component.

To reduce the complexity of the low-temperature spectrum, high temperature data collection performed on the samples allowed more information obtained from the spectrum above. This is due to the fact that at high temperature, the $(3Fe\text{-}4S)^{+}$ cluster exhibits a single quadrupole doublet (Huynh and Kent, 1984), and this doublet is similar to that of a $(2Fe\text{-}2S)^{2+}$ cluster since both clusters are composed of only Fe (III) S_4 units. As

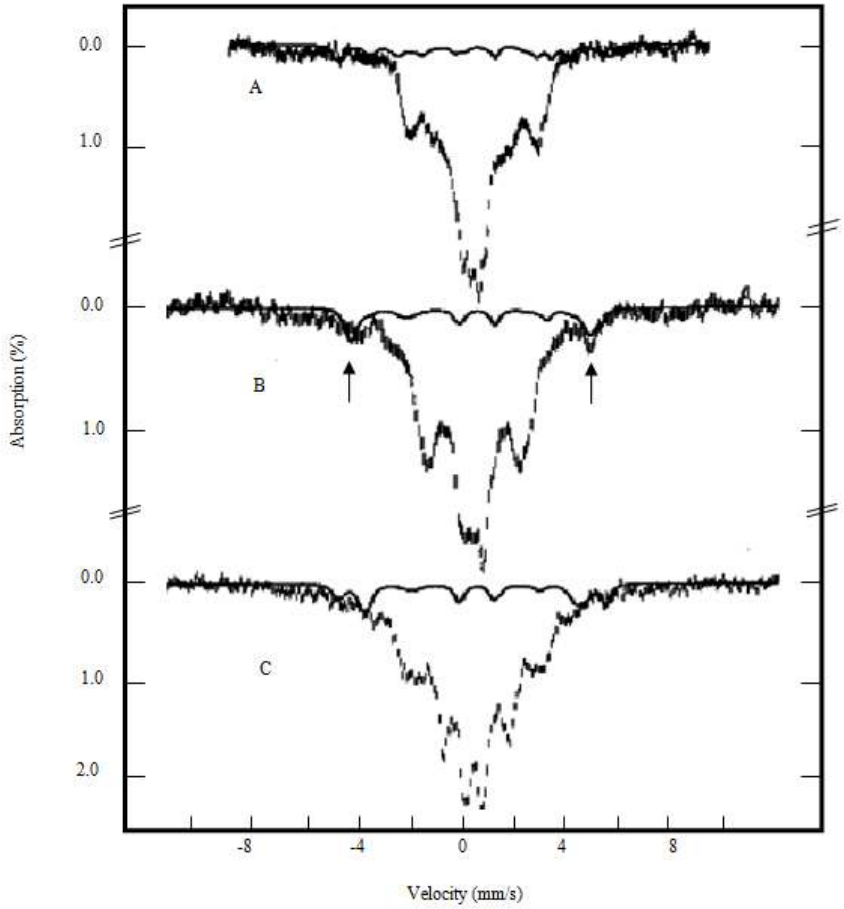

Fig. 14: Mössbauer spectra of an aerobically purified native PFL-AE where contributions from the $(4Fe\text{-}4S)^{2+}$ (8%) and $(2Fe\text{-}2S)^{2+}$ (12%) clusters removed
Mössbauer spectra of an aerobically purified native PFL-AE where contributions from the $(4Fe\text{-}4S)^{2+}$ (8%) and $(2Fe\text{-}2S)^{2+}$ (12%) clusters have been removed; The spectra were recorded at 4.2 K in a parallel field of 50 mT (A), in a parallel field of 4 T (B), or 8 T (C); The solid lines shown in A, B, and C are theoretical simulations of the linear $(3Fe\text{-}4S)^{+}$ cluster; The arrows in B indicate the positions at which the outermost lines of the three Fe sites of the linear $(3Fe\text{-}4S)^{+}$ cluster overlap at 4 T

expected, the 170 K spectrum of the as-isolated PFL-AE (Fig. 13B) shows predominantly a quadrupole doublet arising from both the $(3Fe\text{-}4S)^{+}$ and $(2Fe\text{-}2S)^{2+}$ clusters (dashed line in Fig. 13B) and the central doublet accounts for 80% of the total Fe absorption, consistent with the sum of the amounts of these two types of clusters determined at 4.2 K. The presence of a small quantity of the $(4Fe\text{-}4S)^{2+}$ cluster is supported by the appearance of a shoulder at the high-energy line of the central doublet. Simulation of the $(4Fe\text{-}4S)^{2+}$ cluster using the parameters determined from the dithionite-reduced sample and normalized to 8% of the total Fe absorption yields the solid line overlaid with the experimental data.

The fourth spectral component is readily observed in a spectrum recorded at 4.2 K in a parallel field of 4 T (Fig. 14B). This component is seen as a magnetic spectrum with its outermost lines appearing at approximately -5 and 5 mm/sec (indicated by arrows), which in a much weaker (0.05 T) or stronger (8 T) applied field (Fig. 14, spectra A and C, respectively), becomes broad and is difficult to detect. The field-strength dependence and the observed magnetic splitting are consistent with those of a linear $(3Fe\text{-}4S)^{+}$ cluster (Kennedy *et al*., 1987, 1984; Girerd *et al*., 1984). For a linear $(3Fe\text{-}4S)^{+}$ cluster, the three $S = 5/2$Fe (III) sites are spin-coupled to form an $S = 5/2$ ground state. The spin of the middle Fe site (site 3) is ant parallel to those of the two terminal Fe sites (sites 1 and 2). Consequently, the internal field of site 3 is parallel to the applied field, while those of the other two sites oppose the applied field.

Comparing the results obtained for the linear $(3Fe\text{-}4S)^{+}$ cluster in aconitase (Kennedy *et al*., 1987) with the PFLA-E spectra, the observed internal fields for sites 1, 2 and 3 in aconitase are -33.6, -31.9 and 24.2 T, respectively. The signs indicate the direction of the internal field in relation to that of the applied field. At 0.05 T, since all three internal fields are different in magnitude, the spectra arising from the three Fe sites

show different magnetic splittings. Superposition of these three spectra results in a relatively broad spectrum (solid line overlaid with the experimental spectrum in Fig. 14A). At 4T, to a good approximation, the magnitudes of the effective fields at sites 1 and 2 are reduced by 4 T to 29.6 and 27.9 T, respectively, while that of site 3 is increased to 28.2 T. These values are quite similar and thus, all three sites show similar magnetic spectra, superposition of which results in a "single" magnetic spectrum with its intensity tripled (solid line in Fig. 14B). At 8 T, the magnitudes of the effective fields at sites 1, 2 and 3 are again different and a broad magnetic spectrum is again observed (solid line in Fig. 14C). On the basis of the above analysis, it is concluded that the as-isolated PFL-AE contains linear $(3Fe\text{-}4S)^{+}$ clusters, accounting for approximately10% of the total iron absorption.

ENDOR: The electron-nuclear couplings are an important parameter in the investigation of paramagnetic systems in order to obtain information on the ligand coordinates. However, the couplings of the electron spins to many surrounding nuclear spins may lead to a low resolution of the EPR spectrum due to line broadening and line splitting effects. These interactions are also usually too small to be resolved within the line width of the EPR line. NMR techniques cannot be directly employed to obtain the electron-nuclear couplings either because of the greatly increased line widths caused by the presence of the unpaired electron. However, this problem can be eliminated by performing a double resonance experiment which detects the NMR resonances via intensity changes of a simultaneously irradiated EPR line. The Electron Nuclear Double Resonance (ENDOR) experiment, detects the NMR quanta in the microwave rather than the RF range (known as quantum transformation) resulting in a sensitivity enhancement of several orders of magnitude over conventional NMR spectroscopy. ENDOR can therefore be regarded as NMR-detected EPR spectroscopy (Murphy and Farley, 2006).

ENDOR offers many advantages, compared to EPR in terms of structural characterization of paramagnetic systems in solution and in the solid state. One very important advantage of the technique is the resolution enhancement gained for organic radicals in solution. In general, each group of equivalent nuclei (regardless of how many nuclei belong to this group) contributes only two lines to the ENDOR spectrum. Addition of nonequivalent nuclei to the paramagnetic system causes a multiplicative increase in the number of lines in the EPR spectrum. In contrast, this results to an additive increase in the ENDOR spectrum. Furthermore, since each ENDOR resonance is centered about the field dependent nuclear Larmor frequency of the nucleus, exact identification of the interacting nucleus can be obtained (Murphy and Farley, 2006).

Another major advantage of the ENDOR technique is the ability to obtain structural information from the powder EPR spectra of metal complexes or paramagnetic proteins in frozen solution. The most sensitive probe for structure determination is the electron nuclear hyperfine interaction tensor and this can be obtained using ENDOR spectroscopy. The frozen solution EPR spectrum (or powder spectrum) is composed of a superimposition of the individual resonances from the randomly oriented molecules in which the applied magnetic field assumes all possible orientations with respect to the molecular frame. ENDOR measurements made at a selected field position in the EPR spectrum comprise only that subset of molecules having orientations that contribute to the EPR intensity at the chosen value of the observing field. However, careful selection of magnetic field values which correspond to defined molecular orientations can be obtained and in this ''angular selective'' or ''orientation selective'' ENDOR experiment, the principal components of the magnetic tensors for each interacting nucleus can be obtained by simulation of the data. Information obtained from this field dependent experiment can be used to provide structural information on the distance and spatial orientation of the remote nucleus. This ability to obtain three dimensional structures is extremely important for paramagnetic system slacking long range order or in cases where single crystals cannot be prepared.

ENDOR can be performed either in a CW or time-domain (pulsed) mode, which may require a few considerations. CW ENDOR of metalloenzymes almost always has better sensitivity than pulsed because in general a microwave pulse cannot flip all the electron spins in a sample. Conversely, pulsed ENDOR often gives better line shapes/resolution and the ability to vary pulse sequences and manipulate polarizations/coherences in pulsed ENDOR provides its own benefits (Schweiger, 1991; Doan and Hoffman, 1997).

Basic principles of ENDOR spectroscopy: ENDOR was introduced for solids by Feher in 1956 and later by Hyde and Maki for liquids and is considered the oldest and most widely used multiple resonance technique. In a simple EPR experiment, one frequency (microwave) is used to excite the EPR transition while in a multiple resonance experiment, two or more irradiating fields are used to excite different transitions simultaneously. In ENDOR, one monitors the effects on an EPR transition of a simultaneously excited NMR transition and thus one essentially detects the NMR absorption with much greater inherent sensitivity than EPR. To explain how the technique works, let us consider the appropriate energies for the simplest case of a two spin system (i.e., one electron and one proton) interacting with an applied magnetic field (Fig. 15). The simplified spin Hamiltonian for this two spin system ($S = 1/2$, $I = 1/2$) in an external applied field B_0 is given as:

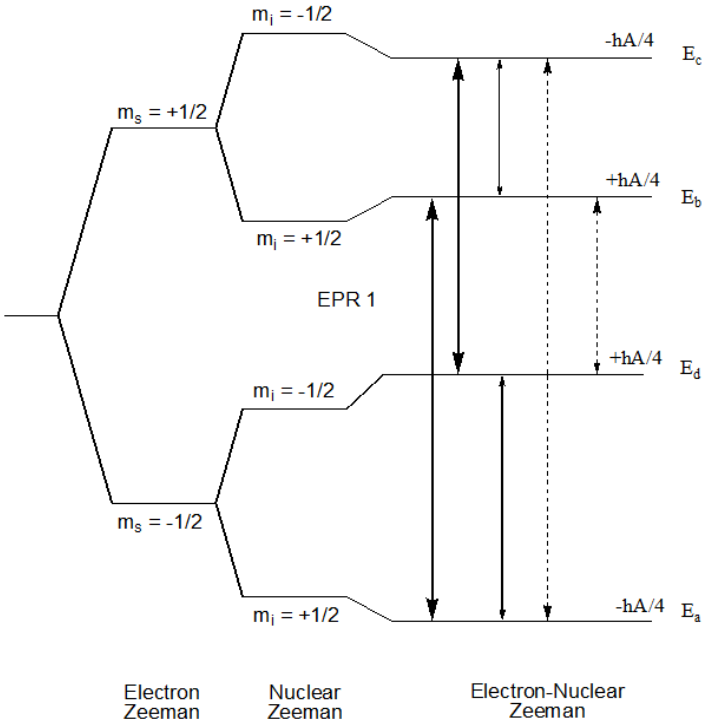

Fig. 15: ENDOR energy level diagram for an S = 1/2, I = 1/2 spin system
Energy level diagram for an S = 1/2, I = 1/2 spin system assuming the g-value and hyperfine coupling are isotropic; The bold lines show the allowed EPR transitions; the solid lines are the ENDOR transitions and the dashed lines; the EPR "semiforbidden" transition

$$H = H_{EZ} + H_{NZ} + H_{HFS} \quad (19)$$

where,
EZ = Electron Zeeman term
NZ = Nuclear Zeeman term
HFS = Hyperfine interaction

This equation takes the form:

$$H = \mu_B B_0 \cdot g \cdot S - 2\, g_n \mu_n n B_0 \cdot I + hS \cdot A \cdot I \quad (20)$$

where, g_n is the nuclear g-factor, S and I are the vector operators of the electron and nuclear spins, μ_B (commonly written as β_e in the literature) is the Bohr magneton (9.274 610224 J/T), μ_n is the nuclear magneton (5.05×10^{-27} J/T), h is the Planck constant (6.626×10^{-34} J s) and g and A are the g- and hyperfine coupling tensors. Assuming only isotropic interactions and with the external magnetic field aligned along the Z axis, the following expression is obtained:

$$H = g\mu_B B_0 S_Z - g_n \mu_n B_0 I_Z + haS \cdot I \quad (21)$$

where, g is the dimensionless isotropic g-factor and a is the isotropic hyperfine coupling constant in Hertz (Hz), not to be confused with $A/g u_B$which is the hyperfine splitting in field units. Ignoring second order terms and in the high field approximation, the energy levels for the two spin system (S = 1/2, I = 1/2) can be defined as:

$$E(M_S, M_I) = g\mu_B B_0 M_S - g_n \mu_n B_0 M_I + haMSMI \quad (22)$$

where, M_S and M_I are the magnetic spin quantum numbers, with values of ±1/2 For simplicity, the electron and nuclear Zeeman energy terms can be expressed in frequency units giving:

$$\frac{E(M_S,M_I)}{h} = \nu_e M_S - \nu_n M_I + aM_S M_I \quad (23)$$

where, $\nu_e = g\mu_B B_0/h$ and $\nu_n = g_n \mu_n B_0/h$. The four possible energy levels resulting from this equation (labelled E_a-E_d) can be written as follows:

$$E_a = -{}^1/_2\, g\mu_B B_0 - {}^1/_2\, g_n \mu_n B_0 - {}^1/_4\, ha \quad (24)$$

$$E_b = +{}^1/_2\, g\mu_B B_0 - {}^1/_2\, g_n \mu_n B_0 + {}^1/_4\, ha \quad (25)$$

$$E_c = +{}^1/_2\, g\mu_B B_0 + {}^1/_2\, g_n \mu_n B_0 - {}^1/_4\, ha \quad (26)$$

$$E_d = -\,{}^1/_2\, g\mu_B B_0 + {}^1/_2\, g_n \mu_n B_0 + {}^1/_4\, ha \quad (27)$$

By application of the EPR selection rules ($\Delta M_I = 0$ and $\Delta M_S = \pm 1$), it is found that two possible resonance transitions can occur, namely ΔE_{cd} (labeled EPR 1) and ΔE_{ab} (labeled EPR 2), as shown in Fig. 12:

$$\Delta E_{cd} = E_c - E_d = g\mu_B B - {}^1/_2\, ha \quad (28)$$

$$\Delta E_{ab} = E_b - E_a = g\mu_B B + {}^1/_2\, ha \quad (29)$$

These two transitions give rise to two absorption peaks at different magnetic field positions and are separated by a, the isotropic hyperfine splitting:

$$\nu_{EPR} = \nu_e \pm a/2 \quad (30)$$

It is these NMR transitions that are detected by ENDOR via the intensity changes to the simultaneously irradiated EPR transition. It is important to note, that both the hyperfine coupling constant (a) and the nuclear Larmor frequencies (ν_n) are determined in the ENDOR experiment. Therefore, unlike the situation in EPR, the hyperfine couplings can be measured with higher resolution and accuracy and can also be directly assigned to a specific nucleus since the values of ν_n are specific to an individual nuclei listed in Table 3. For many nuclei, ν_n values occur at low frequencies (less than 5 MHz) so the assignments are often complicated in multi-nuclear systems due to overlapping signals from different nuclei. Since ν_n is field dependent, it is often beneficial to perform the ENDOR measurements at higher frequencies (e.g., 35 and 90 GHz). For an (S = 1/2, I = 1/2) system, two ENDOR lines are detected which equally spaced about ν_n and separated by the hyperfine coupling constant. This pattern occurs in the case where $\nu_n < |a/2|$. In the case where, $\nu_n > |a/2|$, the energy level diagram must be changed and then two ENDOR lines are observed, centered around a/2 and separated by $2\nu_n$ (Murphy and Farley, 2006).

Because of the long relaxation times of most nuclei, ENDOR spectra tend to be sharper than the original EPR transition. This allows the detection of hyperfine splittings that were previously undetectable in the EPR spectrum. This technique has been especially helpful in interpreting EPR spectra of metalloproteins which often possess broad lines due to unresolved hyperfine structure.

ENDOR determination of the active site: The derivation of bonding and geometric information starts with the determination of the hyperfine interaction tensor/matrix (Abragam and Bleaney, 1986), A, for a hyperfine-coupled nuclei, along with the quadrupole interaction tensor when I>2. This requires a set of measurements taken over a range of orientations of the

Table 3: Common nuclei used in ENDOR spectroscopy

Nucleus	Abundance (%)	Spin (I)	ν_N/MHz (3.5 kG)	ν_N/MHz (12.5) kG
^{1}H	99.9850	½	14.902180	53.222070
^{2}H	0.0148	1	5.585691	19.948890
^{13}C	1.1100	½	3.747950	13.385530
^{14}N	99.6300	1	1.077201	3.847146
^{15}N	0.3660	½	1.511052	5.396614
^{17}O	0.0380	5/2	2.020990	7.217820

Nuclear spin quantum numbers and nuclear larmor frequencies at X-band (9 GHz) and Q-band (35 GHz)

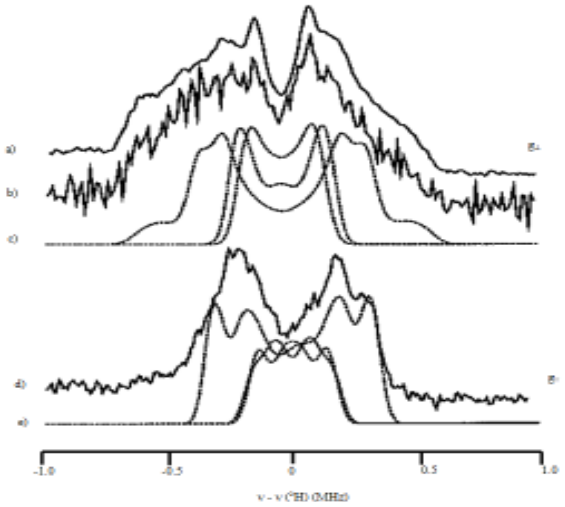

Fig. 16: Q-band mims pulsed-ENDOR field dependence spectra of PFL-AE with methyl-D_3-AdoMet
Q-band mims pulsed-ENDOR spectra of PFL-AE with methyl-D_3-AdoMet; (a) and (d) photoreduced sample, (b) cryoreduced sample, spectra (c) and (e) are simulations (dashed lines) with dipolar tensors; The spectra at $g_\perp$ have been scaled to the height of the natural abundance ^{57}Fe peaks visible to higher frequency of the ^{13}C signals; Conditions: T = 2 K, microwave frequency = 34.8 GHz, microwave pulse lengths = 80 ns, τ = 456 ns, RF pulse length = 60 us, repetition rate = 30 Hz

molecular frame relative to the external field. The samples employed in ENDOR studies of metalloenzymes almost always are frozen solutions which contain a random distribution of active-site orientations. This could prove to be problematic in terms of obtaining the required "orientational" dataset but this concern can be addressed by analyzing a "2-D" pattern comprised of "orientation-selective" ENDOR spectra collected at multiple fields (g-values) across the EPR envelope of a frozen solution sample (DeRose and Hoffman, 1995).

The hyperfine matrix obtained for a particular nucleus can be decomposed into two components: $A = A_{loc}+T$. The "local" contribution, A_{loc}, arises from spin on the atom whose nucleus is observed. The term arises from covalent (through-bond) interactions within the paramagnetic catalytic center and generally is announced by the presence of an isotropic (s-orbital) hyperfine coupling. The complete set of nuclei that exhibit an A_{loc} component thus gives the composition of the covalent network that incorporates the metal ion, which includes but is not limited to the coordination sphere of the metal ion(s) (Hoffman, 2003). For atoms involved in the covalent network, detailed analysis of A_{loc} (and the quadrupolar tensor) can yield the valence of the metal ions, covalency parameters for ligands, as well as the coordination geometry of the metal center (Lee *et al*., 1997; Manikandan *et al*., 2001).

Atoms that are not covalently linked but are near to the active site still exhibit a "nonlocal", dipolar coupling to the electron spin, T (Hutchison and McKay, 1977). Analysis of their coupling yields the coordinates of those atoms. Overall, determination of the positions for several atoms of a bound substrate, product, or inhibitor can provide enough geometric constraints to define its structure. However, this information is most richly interpretable in the context of a related crystal structure (Hoffmann, 2003).

Interaction of SAM to the Fe-S cluster of PFL-AE: The archetypal (4Fe-4S) cluster of aconitase, which isomerizes citrate to isocitrate is distinct in having a unique Fe ion which is not coordinated to the enzyme by a cysteinyl sulfur. The obvious role of such an Fe is a catalytic one and indeed, the aconitase cluster isomerizes citrate/isocitrate through a mechanism in which the reactant/product is chelated to the unique cluster Fe (Werst *et al*., 1990; Kennedy *et al*., 1987). Using the aconitase system as the model, an alternative role for the unique Fe of the (4Fe-4S) cluster of the Pyruvate Formate-Lyase Activating Enzyme (PFL-AE) was demonstrated.

^{2}H and ^{13}C pulsed ENDOR spectroscopy was performed by Walsby *et al*. (2002a) on $(4Fe\text{-}4S)^{+}$-PFL-AE (S = 1/2) with bound labeled AdoMet (denoted (1+/AdoMet)) at the methyl position labeled with either ^{2}H or ^{13}C. The observation of substantial ^{2}H and ^{13}C hyperfine couplings from the labels clearly demonstrated that AdoMet binds adjacent to the 4Fe cluster. The ^{2}H spectra of (1+/CD_3-AdoMet) taken at $g_{\perp}$ and $g_{\parallel}$ both show a well-defined deuterium pattern (Fig. 16). The breadth of the signal collected at $g_{\perp}$ is 1.1 MHz, which, when corrected for unresolved ^{2}H quadrupole splitting of ~0.1 MHz based on the known value for quadrupole coupling for CD_3 (Ragle *et al*., 1975). This corresponds to a substantial ^{1}H coupling of ~6-7 MHz and for comparison, this coupling is approximately half that of water bound to a low-spin heme (Fann *et al*., 1994).

The cofactor was shown to bind in the same geometry to both the 1+ and 2+ states of the cluster. The interactions between AdoMet and the diamagnetic $(4Fe\text{-}4S)^{2+}$ state was determined by preparing a $(4Fe\text{-}4S)^{2+}$ PFL-AE sample that is first frozen in the presence of AdoMet and then γ-irradiated at 77 K to produce the $(4Fe\text{-}4S)^{+}$ valency cluster cryogenically trapped in the geometry of the 2+ state, denoted $(2+/AdoMet)_{red}$. As shown, the ^{2}H spectra of (1+/CD_3-AdoMet) and $(2+/CD_3\text{-AdoMet})_{red}$ are indistinguishable as seen in Fig. 16.

^{13}C ENDOR spectra collected from (1+/$^{13}CH_3$-AdoMet) and $(2+/^{13}CH_3\text{-AdoMet})_{red}$ led to identical conclusions where the two labeled samples exhibit identical hyperfine-split doublets centered at the ^{13}C Larmor frequency (Fig. 17). The doublet arises from coupling to ^{13}C of the labeled AdoMet lying adjacent to the cluster. ENDOR signals from natural abundance ^{57}Fe were also observed assigned to the ν_{+} transition of a single iron with a coupling of A (^{57}Fe) = 26 MHz, which is similar to that of the labile Fe site in aconitase, A (^{57}Fe) = 29 MHz. This additional signal provided a method for normalizing spectra from natural abundance and ^{13}C-enriched samples, by scaling to the ^{57}Fe signal. Analysis of the data disclosed a through-bond (local), isotropic contribution to the ^{13}C interaction, which requires overlap between orbitals on the cluster and on AdoMet. The most plausible origin is a dative interaction of the positively charged sulfur of AdoMet with a negatively charged sulfide of the cluster, rather than with the unique Fe of the cluster. These results led to a proposed reaction mechanism in which inner-sphere electron transfer from the cluster to AdoMet via the sulfide-sulfonium interaction causes cleavage of the sulfonium-adenosyl bond (Walsby *et al*., 2002a).

Modeling of the through-space electron-nuclear dipolar interaction between the cluster electron spin and the methyl-^{13}C and ^{2}H of AdoMet is derived from orientation-selective, 2-D ENDOR datasets. The intervening deuterium spectra show that the breadth of the pattern decreases monotonically from $g_{\perp}$ to $g_{\parallel}$. Although not highly resolved, the hyperfine splitting at $g_{\perp}$ is roughly twice that of the splitting at $g_{\parallel}$. For a CD_3 moiety, the maximum ^{2}H quadrupole coupling is only

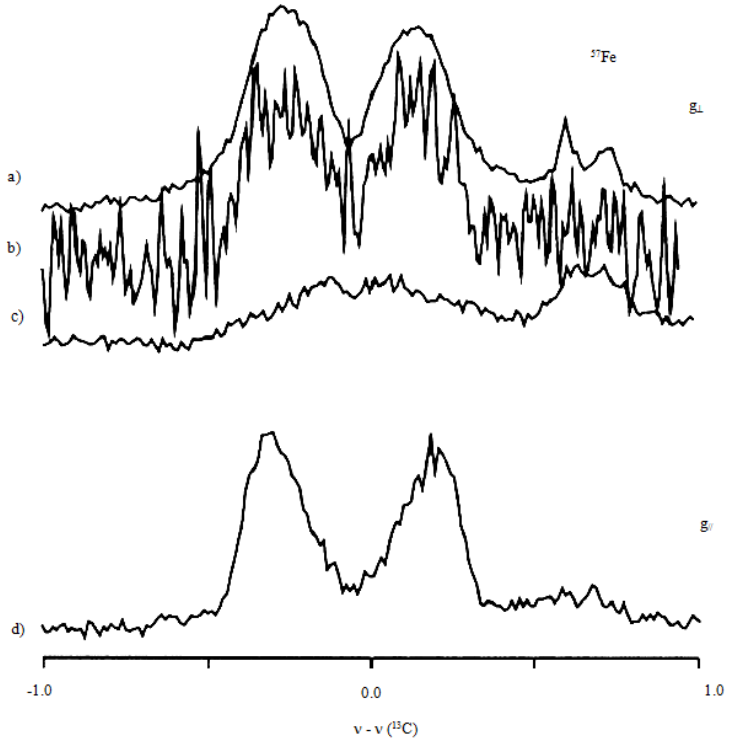

Fig. 17: Q-band ^{13}C ENDOR spectra of PFL-AE with methyl-^{13}C-AdoMet
Q-band mims pulsed-ENDOR spectra of PFLAE (a) with methyl-^{13}C-AdoMet, photoreduced, at $g_{\perp}$, (b) with methyl-^{13}C-AdoMet, (d) with methyl-^{13}C-AdoMet, photoreduced, at $g_{//}$|. Irradiatedat 77 K, at $g_{\perp}$ (c) with natural abundance ^{13}C-AdoMet at $g_{//}$; Experimental conditions similar to Fig. 16 except that τ = 600 ns

P~0.1 MHz[53] and for a ^{2}H spectrum as broad as that shown in (Fig. 16), the shape is dominated by the hyperfine interaction to the three deuterons (*j* = 1-3). The spectra are compatible with a surprisingly simple model in which the AdoMet is bound alongside the cluster and the outer features of the CD_3 ENDOR response are governed by the through-space dipolar interaction between the closest methyl deuteron and the spin density on a single Fe ion of the cluster; the inner part of the pattern is filled in by intensity from the other two methyl-group deuterons. The analysis showed that the shortest distance between an AdoMet methyl proton and an iron of the cluster is ~3.7 Å (Abragam and Bleaney, 1986), with a distance of ~4.9 Å (Lowe, 1995) from the methyl carbon to this iron.

The 2D pattern of the^{13}C ENDOR spectra from (1+/$^{13}CH_3$-AdoMet) collected across the entire EPR envelope showed that the ^{13}C tensor can be decomposed into the sum of an isotropic part and two, mutually perpendicular dipolar tensors (Fig. 18). The former was assigned to the through space dipolar interaction between the ^{13}C and spin of the cluster; the latter we assign to the "local" interaction with the spin on the ^{13}C itself whose presence is disclosed by the isotropic term. The hyperfine tensor, thus, can be decomposed into the "nonlocal" dipolar interaction with the cluster and a "local" term that arises from spin density on the ^{13}C. The presence of spin density at the methyl group of AdoMet, as manifest in this local term, requires that AdoMet lie in contact with the cluster, weakly interacting with it through an incipient bond/antibond. The opposite signs of the through-space and local contributions suggests that the spin on the methyl carbon is not directly delocalized from the cluster but involves spin polarization through an intervening atom, presumably the sulfonium sulfur of AdoMet (Walsby *et al*., 2002a).

Coordination sphere of the unique iron site: The derived possible mechanism offered no role for the unique cluster iron, although it appeared that the (4Fe-4S) cluster of every enzyme in the Fe-S/AdoMet family has one. To investigate the possibility of AdoMet coordinating to the unique site of the (4Fe-4S) cluster of PFL-AE, isotopically labeled *S*-adenosylmethionine with ^{17}O and ^{13}C at the carboxylate oxygen and with ^{15}N at the amine nitrogen on the amino were prepared. Each labeled SAM was added to photo reduced $(4Fe-4S)^{+}$ -PFL-AE and the solutions were frozen for ENDOR measurements. The observation of ENDOR signals for all three nuclei demonstrated for the first time that SAM forms a classical five-membered chelate ring with the unique iron of the (4Fe-4S) cluster of PFL-AE. The ^{17}O (Fig. 19) and ^{13}C (Fig. 20) couplings

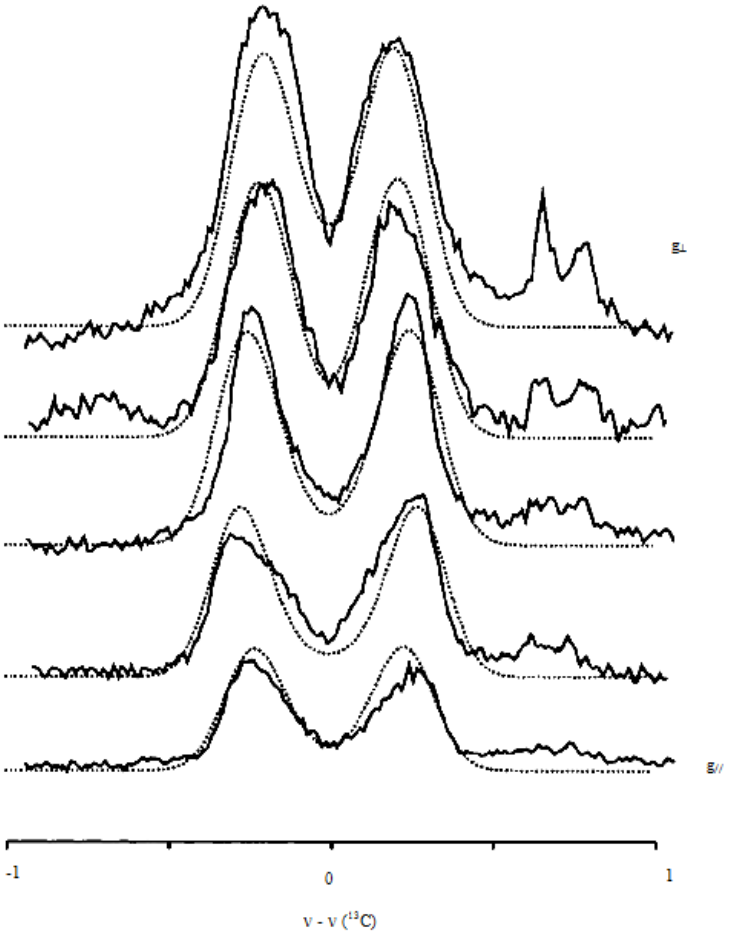

Fig. 18: Q-band ^{13}C ENDOR field dependence spectra of PFL-AE with methyl-^{13}C-AdoMet
Q-band ^{13}C ENDOR field dependence of PFL-AE with methyl-^{13}C-AdoMet with conditions similar to Fig. 17; The dashed lines are simulations with dipolar tensors

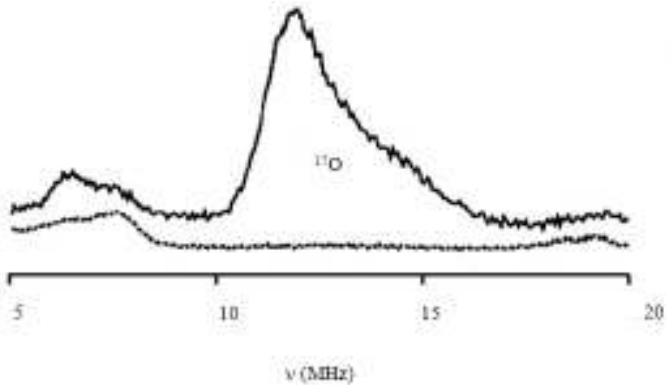

Fig. 19: Q-band pulsed ENDOR of PFL-AE with ^{17}O-carboxylato-AdoMet
Q-band pulsed ENDOR spectra of PFL-AE with ^{17}O-carboxylato-AdoMet conditions: T = 2 K, microwave frequency = 34.9 GHz, radiofrequency pulse length = 60 uS, microwave pulse lengths = 80, 40, 80 ns

observed in the PFL-AE/SAM complex are 12.2 MHz and 0.71 MHz, respectively and are very similar to those found for aconitase with carboxylate-labeled citrate/isocitrate, Fig. 16. The strong couplings support direct coordination of a carboxylate oxygen of SAM to the unique iron in PFL-AE, as also measured in the case of the aconitase enzyme-substrate complex (Kennedy, *et al*., 1987, 1984). The ^{15}N coupling of 5.8 MHz (Fig. 21) is comparable to those observed for ^{15}N ligands similar to the ^{15}N-histidine bound to the Rieske

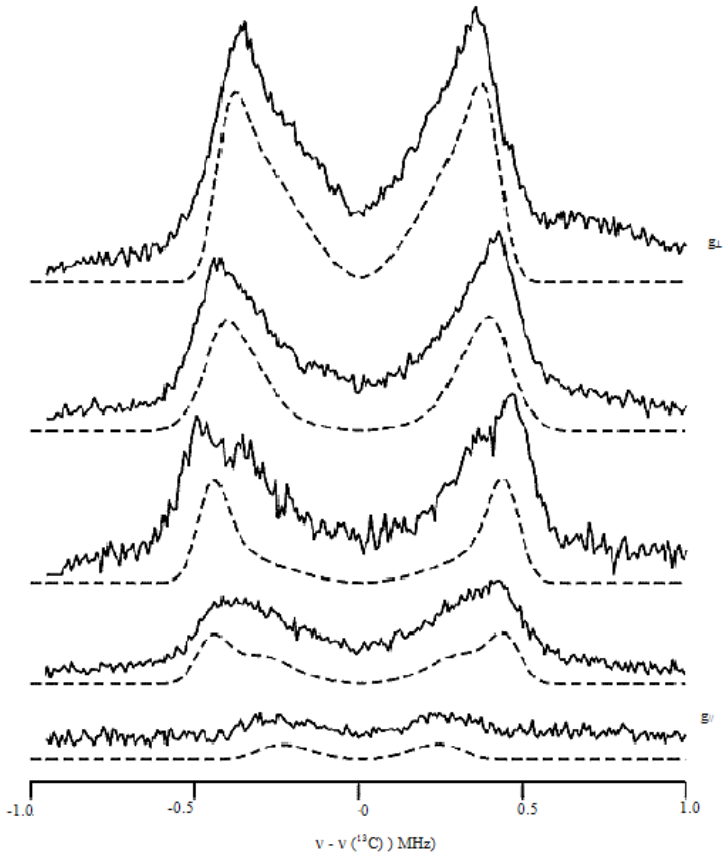

Fig. 20: Q-band ENDOR of PFL-AE with ^{13}C-carboxylato AdoMet field dependence
Field dependence data (solid) and simulations (dashed) from Q-band mims pulsed ENDOR of PFL-AE with carboxy-^{13}C-AdoMet; Conditions are similar to Fig. 21

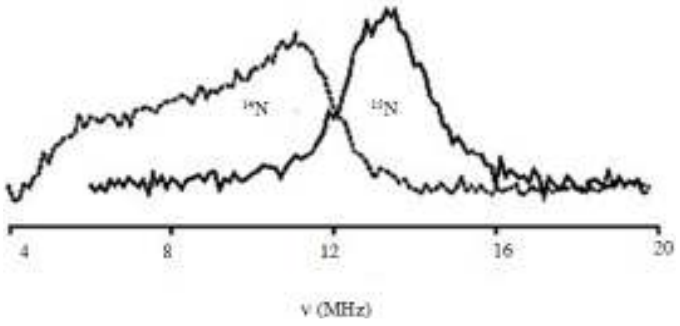

Fig. 21: Q-band ENDOR of PFL-AE with $^{14/15}$N-amino-AdoMet
Q-band pulsed ENDOR of PFL-AE with ^{15}N-amino-AdoMet; Conditions: T = 2 K, microwave frequency = 34.9 GHz, radiofrequency pulse length = 60 uS, microwave pulse lengths = 80, 40, 80 ns

(2Fe-2S) cluster (Gurbiel *et al*., 1996) and the ^{15}N-ACC (ACC = 1-aminocyclopropane-1-carboxylic acid) coordinated to the non-heme iron of itsoxidase ACCO (Rocklin *et al*., 1999), both of which involve direct coordination. The results obtained therefore unambiguously establish the function of the unique Fe site and provides the first direct spectroscopic evidence for a direct interaction between AdoMet and the (4Fe-4S)$^{+}$ cluster of PFL-AE.

Coordination of the methionine portion of SAM to the unique iron of the (4Fe-4S) cluster of PFL-AE is intriguing, as it suggests that the unique iron serves as an anchor to hold the cosubstrate SAM in place for reaction. The relevant part of SAM, however, is the sulfonium, as it is the S-C (5') bond that is reductively cleaved in catalysis and so considerable interest in investigating the proximity of this moiety to the cluster is imperative. The results of the ENDOR spectroscopy taken together, provided a working model for SAM

binding in which the methionine portion of SAM serves to anchor the co-substrate in place by coordination to the unique site of the cluster such that the sulfonium sulfur is in close contact with one of the u_3-bridging sulfides of the cluster; this close contact is proposed to provide the pathway for inner-sphere electron transfer from the cluster to SAM to initiate the radical reaction.

CONCLUSION

The spectroscopic results presented herein provide significant insight into the mechanism by which PFLAE and more generally, all of the radical-SAM enzymes, presumably initiate radical catalysis using an iron-sulfur cluster and *S*-adenosylmethionine. Analysis of the Mössbauer data of the as-isolated PFL-AE shows the presence of mixtures of Fe-S clusters. A majority of the clusters are present in the cuboidal $(3Fe\text{-}4S)^{+}$ state (~0.29 cluster/protein monomer), while minor portionsare in the $(2Fe\text{-}2S)^{2+}$ (~0.08 cluster/monomer), $(4Fe\text{-}4S)^{2+}$ (~0.03 cluster/monomer) and linear $(3Fe\text{-}4S)^{+}$ (~0.04 cluster/monomer) states.

EPR-detected single-turnover experiments have illustrated that PFL-AE utilizes a reduced $(4Fe\text{-}4S)^{+}$ cluster in catalysis and this cluster is the source of the electron required for reductive cleavage of AdoMet and subsequent generation of the glycyl radical in PFL. Mössbauer spectroscopy was again used to identify a unique iron site in the (4Fe-4S) cluster of PFL-AE, while ENDOR spectroscopy showed that AdoMet coordinates to this unique iron via a classic five-member amino acid chelate ring in both the oxidized $(4Fe\text{-}4S)^{2+}$ and reduced $(4Fe\text{-}4S)^{+}$ states. ENDOR spectroscopy also demonstrated the close proximity of the sulfonium moiety to the cluster in both oxidation states.

The proposed mechanism outlined in Fig. 22 shows AdoMet binding to the oxidized $(4Fe\text{-}4S)^{2+}$ cluster of PFL-AE via coordination of the unique site, which puts the sulfonium in orbital overlap with one of the $\mu 3$-bridging sulfides of the $(4Fe\text{-}4S)^{2+}$ cluster. One-electron reduction (mediated by reduced flavodoxin in vivo) provides the reduced $(4Fe\text{-}4S)^{+}$ cluster complexed to AdoMet. This $(4Fe\text{-}4S)^{+}$ -SAM complex is stable in the absence of the substrate PFL; however, in the presence of PFL, inner-sphere electron transfer from the $(4Fe\text{-}4S)^{+}$ cluster to the sulfonium of AdoMet initiates homolytic S-C (5') bond cleavage. The resulting methionine is left bound to the unique site of the oxidized $(4Fe\text{-}4S)^{2+}$ cluster, while the adenosyl radical intermediate abstracts the pro-*S* H from G734 of PFL. The catalytic cycle is completed upon displacement of methionine and 5'-deoxyadenosine with an AdoMet cosubstrate. It is of interest to note that recent synthetic models of the radical-SAM enzymes based on site-differentiated (4Fe-4S) clusters have provided evidence for reductive cleavage of sulfonium moieties by reduced (4Fe-4S) clusters, although a stable synthetic cluster-sulfonium complex has not yet been reported (Daley and Holm, 2001, 2003).

The past 10 years have seen an explosion in interest in the enzymes now known to comprise the radical-SAM superfamily. These enzymes catalyze a

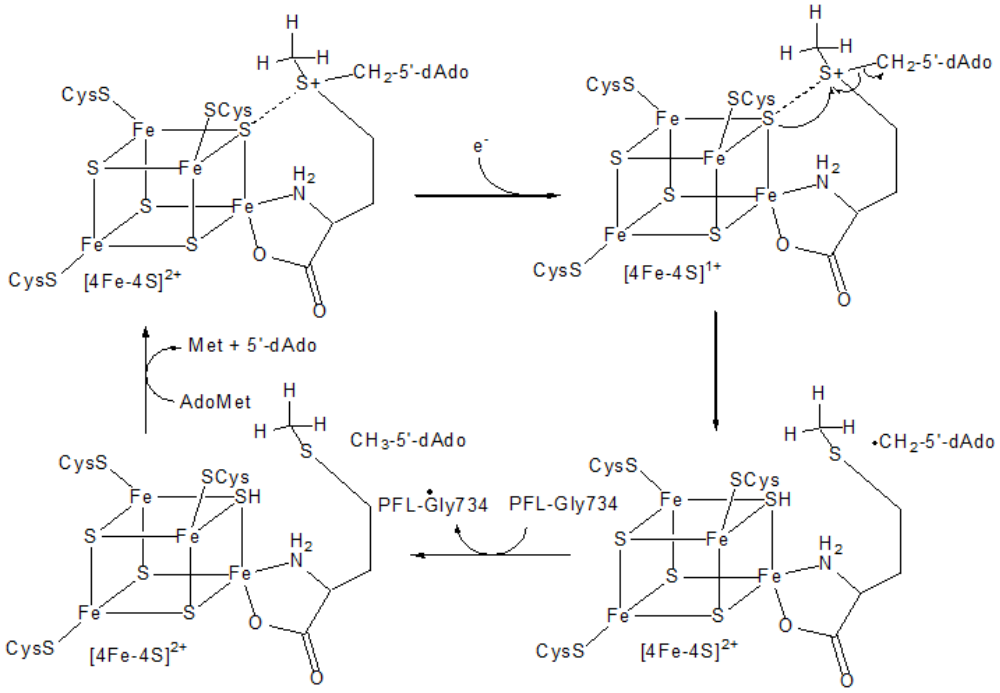

Fig. 22: Iron-sulfur cluster and SAM-mediated radical generation
Proposed mechanism for the iron-sulfur cluster and AdoMet-mediated radical generation catalyzed by PFL-AE

diverse set of reactions, all of which are initiated by H atom abstraction. The evidence for adenosyl radical intermediates in some of these reactions led to early speculation of similarities to B12-catalyzed radical reactions, the classic example of adenosylradical-mediated reactions in biology. However, the evidence to date points to novel chemistry utilized by the radical-SAM enzymes to generate adenosyl radical intermediates. This chemistry has at its core the use of a site-differentiated (4Fe-4S) cluster to coordinate and activate *S*-adenosylmethionine for reductive cleavage. Although many questions remain regarding the detailed mechanisms of these fascinating enzymes, it is clear that these ubiquitous enzymes are revealing new insights into the chemistry of iron-sulfur clusters.

REFERENCES

Abragam, A. and B. Bleaney, 1986. Electron Paramagnetic Resonance of Transition Ions. Dover Publications, New York.

Beinert, H., 2000. Iron-sulfur proteins: Ancient structures, still full of surprises. J. Biol. Inorg. Chem., 5(1): 2-15.

Berg, J.M. and R.H. Holm, 1982. Structures and Reactions of Iron-sulfur Protein Clusters and their Synthetic Analogues. In: Spiro, T.G. (Ed.), Iron-sulfur Proteins. John Wiley and Sons Inc., New York, pp: 1-66.

Broderick, J.B., T.F. Henshaw, J. Cheek, K. Wojtuszewski, S.R. Smith, M.R. Trojan, R.M. McGhan, A. Kopf, M. Kibbey and W.E. Broderick, 2000. Pyruvate formate-lyase-activating enzyme: Strictly anaerobic isolation yields active enzyme containing a $[3Fe\text{-}4S]^{+}$ cluster. Biochem. Bioph. Res. Co., 269(2): 451-456.

Cheek, J. and J.B. Broderick, 2001. Adenosylmethionine- dependent iron-sulfur enzymes: Versatile clusters in a radical new role. J. Biol. Chem., 6(3): 209-226.

Conradt, H., M. Hohmann-Berger, H.P. Hohmann, H.P. Blaschkowski and J. Knappe, 1984. Pyruvate formate-lyase (inactive form) and pyruvate formate-lyase activating enzyme of Escherichia coli: Isolation and structural properties. Arch. Biochem. Biophys., 228(1):133-142.

Daley, C.J.A. and R.H. Holm, 2001. Reactivity of $[Fe_4S_4(SR)_4]^{2-,3-}$ clusters with Sulfonium Cations: Analogue reaction systems for the initial step in biotin synthase catalysis. Inorg. Chem., 40(12): 2785-2793.

Daley, C.J.A. and R.H. Holm, 2003. Reactions of site-differentiated $[Fe_4S_4]^{2+,1+}$ clusters with sulfonium cations: Reactivity analogues of biotin synthase and other members of the S-adenosylmethionine enzyme family. J. Inorg. Biochem., 97(3): 287-298.

DeRose, V.J. and B.M. Hoffman, 1995. Protein structure and mechanism studied by electron nuclear double resonance spectroscopy. Method. Enzymol., 246: 554-589.

Doan, P.E. and B.M. Hoffman, 1997. Making hyperfine selection in Mims ENDOR independent of deadtime. Chem. Phys. Lett., 269(3-4): 208-214.

Drago, R.S., 1977. Physical Methods in Chemistry. Saunders College Publishing, Orlando.

Fann, Y.C., N.C. Gerber, P.A. Osmulski, L.P. Hager, S.G. Sligar and B.M. Hoffman, 1994. ENDOR determination of Heme ligation in chloroperoxidase and comparison with cytochrome P-450Cam. J. Am. Chem. Soc., 116(13): 5989-5990.

Ferreira, G.C., R. Franco, S.G. Lloyd, A.S. Pereira, I. Moura, J.J. Moura and B.H. Huynh, 1994. Mammalian ferrochelatase: A new addition to the metalloenzyme family. J. Biol. Chem., 269(10): 7062-7065.

Frey, P.A., 2001. Radical mechanisms of enzymatic catalysis. Annu. Rev. Biochem., 70: 121-148.

Girerd, J.J., G.C. Papaefthymiou, A.D. Watson, E. Gamp, K.S. Hagen, N. Edelstein, R.B. Frankel and R.H. Holm, 1984. Electronic properties of the linear antiferromagnetically coupled clusters $[Fe_3S_4(SR)_4]^{3-}$, structural isomers of the iron-sulfur (1+) ($[Fe_3S_4]^{1+}$) unit in iron-sulfur proteins. J. Am. Chem. Soc., 106(20): 5941-5947.

Gurbiel, R.J., P.E. Doan, G.T. Gassner, T.J. Macke, D.A. Case, T. Ohnishi, J.A. Fee, D.P. Ballou and B.M. Hoffman, 1996. Active site structure of rieske-type proteins: Electron nuclear double resonance studies of isotopically labeled phthalate dioxygenase from *Pseudomonas cepacia* and Rieske protein from *Rhodobacter capsulatus* and molecular modeling studies of a Rieske center. Biochemistry, 35(24): 7834-7845.

Hagen, K.S., J.G. Reynolds and R.H. Holm, 1981. Definition of reaction sequences resulting in self-assembly of $[Fe_4S_4(SR)_4]^{2-}$clusters from simple reactants. J. Am. Chem. Soc., 103: 4054-4063

Henshaw, T.F., J. Cheek and J.B. Broderick, 2000. The $[4Fe\text{-}4S]^{1+}$cluster of pyruvate formate-lyase activating enzyme generates the glycyl radical on pyruvate formate-lyase: EPR-detected single turnover. J. Am. Chem. Soc., 122(34): 8331-8332.

Hoffmann, B.M., 2003. ENDOR of metalloenzymes. Acc. Chem. Res., 36(7): 522-529.

Holm, R.H., 1992. Trinuclear cuboidal and heterometallic cubane-type iron-sulfur clusters: New structural and reactivity themes in chemistry and biology. Adv. Inorg. Chem., 38: 1-71.

Hutchison, C.A. and D.B. McKay, 1977. The determination of hydrogen coordinates in lanthanum nicotinate dihydrate crystals by Nd+3-proton double resonance. J. Chem. Phys., 66(8): 3311-3330.

Huynh, B.H. and T.A. Kent, 1984. Mössbauer studies of iron proteins. Adv. Inorg. Biochem., 6: 163-223.

Kennedy, M.C., T.A. Kent, M. Emptage, H. Merkle, H. Beinert and E. Münck, 1984. Evidence for the formation of a linear [3Fe-4S] cluster in partially unfolded aconitase. J. Biol. Chem., 259(23): 14463-14471.

Kennedy, M.C., M. Werst, J. Telser, M.H. Emptage, H. Beinhert and B.M. Hoffman, 1987. Mode of substrate carboxyl binding to the $[4Fe\text{-}4S]^+$ cluster of reduced aconitase as studied by ^{17}O and ^{13}C Electron-nuclear double resonance spectroscopy. P. Natl. Acad. Sci. USA, 84(24): 8854-8858.

Knappe, J., H.P. Blaschkowski, P. Gröbner and T. Schmitt, 1974. Pyruvate formate-lyase of *Escherichia coli*: The acetyl-enzyme intermediate. Eur. J. Biochem., 50(1): 253-263.

Knappe, J., S. Elbert, M. Frey and A.F. Wagner, 1993. Pyruvate formate-lyase mechanism involving the protein-based glycyl radical. Biochem. Soc. T., 21(3): 731-734.

Krebs, C., T.F. Henshaw, J. Cheek, B.H. Huynh and J.B. Broderick, 2000. Conversion of 3Fe-4S to 4Fe-4S clusters in native pyruvate formate-lyase activating enzyme: Mössbauer characterization and implications for mechanism. J. Am. Chem. Soc., 122(50): 12497-12506.

Külzer, R., T. Pils, R. Kappl, J. Hüttermann and J. Knappe, 1998. Reconstitution and characterization of the polynuclear iron-sulfurcluster in pyruvate formate-lyase-activating enzyme. J. Biol. Chem., 273(9): 4897-4903.

Lee, H.I., B.J. Hales and B.M. Hoffman, 1997. Metal-Ion valencies of the FeMo cofactor in CO-inhibited and resting state nitrogenase by ^{57}Fe Q-band ENDOR. J. Am. Chem. Soc., 119(47): 11395-11400.

Lowe, D.J., 1995. ENDOR and EPR of Metalloproteins. R.G. Landes Co., Austin.

Manikandan, P., E.Y. Choi, R. Hille and B.M. Hoffman, 2001. 35 GHz ENDOR characterization of the "Very Rapid" signal of Xanthine Oxidase reacted with 2-hydroxy-6-methylpurine ($^{13}C_8$): Evidence against direct Mo-C_8 interaction. J. Am. Chem. Soc., 123(11): 2658-2663.

Middleton, P., D.P.E. Dickson, C.E. Johnson and J.D. Rush, 1978. Interpretation of the mossbauer spectra of the four-iron ferredoxin from *Bacillus stenrothermophilus.* Eur. J. Biochem., 88(1): 135-141.

Middleton, P., D.P.E. Dickson, C.E. Johnson and J.D. Rush, 1980. Interpretation of the mossbauer spectra of the high-potential iron protein from *Chromatium.* Eur. J. Biochem., 104(1): 289-296.

Murphy, D.M. and R.D. Farley, 2006. Principles and applications of ENDOR spectroscopy for structure determination in solution and disordered matrices. Chem. Soc. Rev., 35: 249-268.

Palmer, G., 2000. Electron Paramagnetic Resonance of Metalloproteins. In: Que, L. Jr. (Ed.), Physical Methods in Bioinorganic Chemistry, University Science Books, Sausalito, CA (USA), pp: 121-186.

Ragle, J.L., M. Mokarram, D. Presz and G. Minott, 1975. Quadrupole coupling of deuterium bonded to carbon. J. Magn. Reson., 20(2): 195-213.

Rocklin, A.M., D.L. Tierney, V. Kofman, N.M.W. Brunhuber, B.M. Hoffman, R.E. Christofferson, N.O. Reich, J.D. Lipscomb and L. Que, Jr., 1999. Role of the nonheme Fe (II) center in the biosynthesis of the plant hormone ethylene. P. Natl. Acad. Sci. USA, 96(14): 7905-7909.

Schünemann, V. and H. Winkler. 2000. Structure and dynamics of biomolecules studied by Mössbauer spectroscopy. Rep. Prog. Phys., 63: 263-353.

Schweiger, A., 1991. Pulsed electron spin resonance spectroscopy: Basic principles, techniques and examples of applications. Angew. Chem. Int. Edit., 30: 265-292.

Sofia, H.J., G. Chen, B.G. Hetzler, J.F. Reyes-Spindola and N.E. Miller, 2001. Radical SAM, a novel protein super family linking unresolved steps in familiar biosynthetic pathways with radical mechanisms: Functional characterization using new analysis and information visualization methods. Nucleic Acids Res., 29(5): 1097-1106.

Trautwein, A.X., E. Bill, E.L. Bominaar and H. Winkler, 1991. Iron-containing proteins and related analogs-complementary Mössbauer, EPR and magnetic susceptibility studies. Struct. Bond. (Berlin), 78: 1-95.

Wagner, A.F., M. Frey, F.A. Neugebauer, W. Schäfer and J. Knappe, 1992. The free radical in pyruvate formate-lyase is located on glycine-734. P. Natl. Acad. Sci. USA, 89(3): 996-1000.

Walsby, C.J., D. Ortillo, W.E. Broderick, J.B. Broderick and B.M. Hoffman, 2002b. An anchoring role for FeS clusters: Chelation of the amino acid moiety of S-adenosylmethionine to the unique iron site of the [4Fe-4S] cluster of pyruvate formate-lyase activating enzyme. J. Am. Chem. Soc., 124(38): 11270-11271.

Walsby, C.J., W. Hong, W.E. Broderick, J. Cheek, D. Ortillo, J.B. Broderick and B.M. Hoffman, 2002a. Electron-nuclear double resonance spectroscopic evidence that s-adenosylmethionine binds in contact with the catalytically active $[4Fe\text{-}4S]^+$ cluster of pyruvateformate-lyase activating enzyme. J. Am. Chem. Soc., 124(12): 3143-3151.

Werst, M.M., M.C. Kennedy, H. Beinert and B.M. Hoffman, 1990. Oxygen-17, proton and deuterium electron nuclear double resonance characterization of solvent, substrate and inhibitor binding to the iron-sulfur $[4Fe\text{-}4S]^+$ cluster of aconitase. Biochemistry, 29(46): 10526-10532.

Wong, K.K., B.W. Murray, S.A. Lewisch, M.K. Baxter, T.W., L. Ulissi-DeMario and J.W. Kozarich, 1993. Molecular properties of pyruvate-formate lyase activating enzyme. Biochemistry, 32(51): 14102-14110.